Title
Subunit cooperation in the Get1/2 receptor promotes tail-anchored membrane protein insertion

Permalink
https://escholarship.org/uc/item/1mt8550s

Journal
Journal of Cell Biology, 220(11)

ISSN
0021-9525

Authors
Chio, Un Seng
Liu, Yumeng
Chung, SangYoon
et al.

Publication Date
2021-11-01

DOI
10.1083/jcb.202103079

Peer reviewed

ARTICLE

Subunit cooperation in the Get1/2 receptor promotes tail-anchored membrane protein insertion

Un Seng Chio[1]*, Yumeng Liu[1]*, SangYoon Chung[2], Woo Jun Shim[1], Sowmya Chandrasekar[1], Shimon Weiss[2,3], and Shu-ou Shan[1]

The guided entry of tail-anchored protein (GET) pathway, in which the Get3 ATPase delivers an essential class of tail-anchored membrane proteins (TAs) to the Get1/2 receptor at the endoplasmic reticulum, provides a conserved mechanism for TA biogenesis in eukaryotic cells. The membrane-associated events of this pathway remain poorly understood. Here we show that complex assembly between the cytosolic domains (CDs) of Get1 and Get2 strongly enhances the affinity of the individual subunits for Get3•TA, thus enabling efficient capture of the targeting complex. In addition to the known role of Get1CD in remodeling Get3 conformation, two molecular recognition features (MoRFs) in Get2CD induce Get3 opening, and both subunits are required for optimal TA release from Get3. Mutation of the MoRFs attenuates TA insertion into the ER in vivo. Our results demonstrate extensive cooperation between the Get1/2 receptor subunits in the capture and remodeling of the targeting complex, and emphasize the role of MoRFs in receptor function during membrane protein biogenesis.

Introduction

Integral membrane proteins comprise >30% of the proteins encoded by the genome and are essential for the proper functioning of biological membranes. The high aggregation propensity of the transmembrane domains (TMDs) on membrane proteins requires sophisticated protein machineries for their efficient targeting and translocation. An important class of membrane proteins is tail-anchored proteins (TAs), defined by a single TMD near the C terminus. TAs comprise up to 5% of the eukaryotic membrane proteome and mediate key cellular functions including vesicle fusion, apoptosis, protein translocation, and quality control (Chartron et al., 2012; Hegde and Keenan, 2011). As their single C-terminal TMDs are buried inside the ribosome exit tunnel until translation termination, TAs cannot engage cotranslational protein targeting machineries, such as the signal recognition particle (SRP), and must instead use a posttranslational mechanism of targeting and insertion (Kutay et al., 1993, 1995).

The best studied pathway for TA biogenesis is the guided entry of TA (GET) pathway in yeast and the homologous TMD recognition complex (TRC) pathway in mammals, which mediates the targeted delivery of an essential class of TAs with highly hydrophobic TMDs to the ER membrane (Chio et al., 2017a). Newly synthesized TAs are relayed, via a cascade of cytosolic chaperones and cochaperones, to the targeting factor Get3 (Cho and Shan, 2018; Wang et al., 2010; Rao et al., 2016; Chio et al.,

2019; Mariappan et al., 2010). Get3•TA is captured by the cytosolic domains (CDs) of the Get1/2 receptor complex at the ER membrane, which further induces the release of TA from Get3 and mediates TA insertion into the ER (Mariappan et al., 2011; Stefer et al., 2011; Wang et al., 2011). The GET pathway is conserved across eukaryotic organisms, and deletion of Get3 homologues causes sensitivity to stress conditions in yeast and embryonic lethality in mice (Mukhopadhyay et al., 2006; Shen et al., 2003; Schuldiner et al., 2008).

Structural, biochemical, and biophysical studies showed that nucleotide, TA substrate, and interaction partners extensively regulate the conformation of Get3 during the targeting cycle. Get3 is an obligate homodimer, and nucleotide binding/release at its ATPase domain induce adjustments at the dimer interface that are amplified into larger movements of the helical domains (Mateja et al., 2009; Suloway et al., 2009). In the cytosol, ATP and Get4/5 induce Get3 into a "closed" conformation in which the helical domains of both Get3 subunits are brought into proximity and form a contiguous hydrophobic groove, which provides a binding site for the TA-TMD (Gristick et al., 2014; Mateja et al., 2015). The TA substrate triggers ATP hydrolysis in Get3 and induces it to sample open conformations, which drives the detachment of Get3•TA from Get4/5 and exposes the Get1/2 binding sites, allowing Get3•TA to interact with the membrane receptor complex (Rome et al., 2013; Chio et al., 2017b).

[1]Division of Chemistry and Chemical Engineering, California Institute of Technology, Pasadena, CA; [2]Department of Chemistry and Biochemistry, University of California, Los Angeles, Los Angeles, CA; [3]Department of Physics, Institute for Nanotechnology and Advanced Materials, Bar-Ilan University, Ramat-Gan, Israel.

*U.S. Chio and Y. Liu contributed equally to this paper; Correspondence to Shu-ou Shan: sshan@caltech.edu.

The membrane-associated events remain one of the least understood aspects of the GET pathway. Both Get1 and Get2 contain three TMDs, which mediate their heterodimerization and together form an "insertase" homologous to YidC that is necessary and sufficient for the insertion of TAs into the ER membrane (Wang et al., 2011; Mariappan et al., 2011; McDowell et al., 2020; Zalisko et al., 2017; Stefer et al., 2011). Both subunits also contain CDs that interact with Get3. Get2CD (residues 1–150) contains two conserved helices rich in basic residues (residues 1–40), which cocrystallized with closed, nucleotide-bound Get3 (Mariappan et al., 2011; Stefer et al., 2011; Kubota et al., 2012). In contrast, Get1CD (located between TM1 and TM2) forms a coiled-coil (cc) that inserts like a wedge at the dimer interface of apo-Get3 and induces Get3 into a wide-open conformation, leading to nucleotide release and disruption of the TA binding site. Get1CD is also sufficient to induce TA release from Get3 at high concentrations (Wang et al., 2011), while a large fragment of Get2CD (residues 1–106) did not induce TA release (Mariappan et al., 2011). These observations led to the current model in which the long, flexible Get2CD mediates the capture of Get3 • TA using its N-terminal helix, whereas Get1CD is responsible for remodeling the conformation of Get3 to induce TA release.

This modular model is largely based on the results of studies using the individual Get1CD or Get2CD. However, the measured binding affinities of Get1CD and Get2CD for the Get3 • TA complex are low, with K_ds in the micromolar range (Rome et al., 2014), whereas the in vivo concentration of Get1/2 is 0.17–0.2 µM (Kulak et al., 2014). This poses questions as to how the targeting complex is efficiently captured at the ER membrane. Using a mini-Get1/2 complex in which Get1CD and Get2CD are fused to oppositely charged α-helices that form a stable cc heterodimer (Wang et al., 2011), pull-down and TA release experiments suggested that the presence of both subunits can enhance the binding of the receptor complex to Get3 (Wang et al., 2011). However, the molecular basis for the potential cooperation between the CDs of the two subunits in the Get1/2 complex remains elusive.

In this work, we studied subunit cooperation in Get1/2 during the capture and remodeling of the Get3 • TA targeting complex using mini-Get1/2, which has been shown to recapitulate the cytosolic functions of the Get1/2 complex (Wang et al., 2011). Quantitative binding assays and single-molecule (sm) fluorescence spectroscopy studies revealed extensive cooperation between Get1CD and Get2CD during the binding and conformational remodeling of Get3 • TA. Unexpectedly, Get2CD also induces Get3 opening. This activity is mediated by two molecular recognition features (MoRFs) in the disordered linker of Get2CD, and their mutations attenuated TA insertion in vivo. Our results identify a mechanistically important step for the membrane-associated events in the GET pathway.

Results

Complex assembly enhances the affinity of the individual Get1/2 CDs for Get3•TA

Mini-Get1/2 was previously used to mimic the function of the CDs of the Get1/2 receptor complex (Fig. S1, A and B; Wang et al., 2011). Mini-Get1/2 coimmunoprecipitated with Get3 more strongly than variants bearing either the N72A/R73E mutation
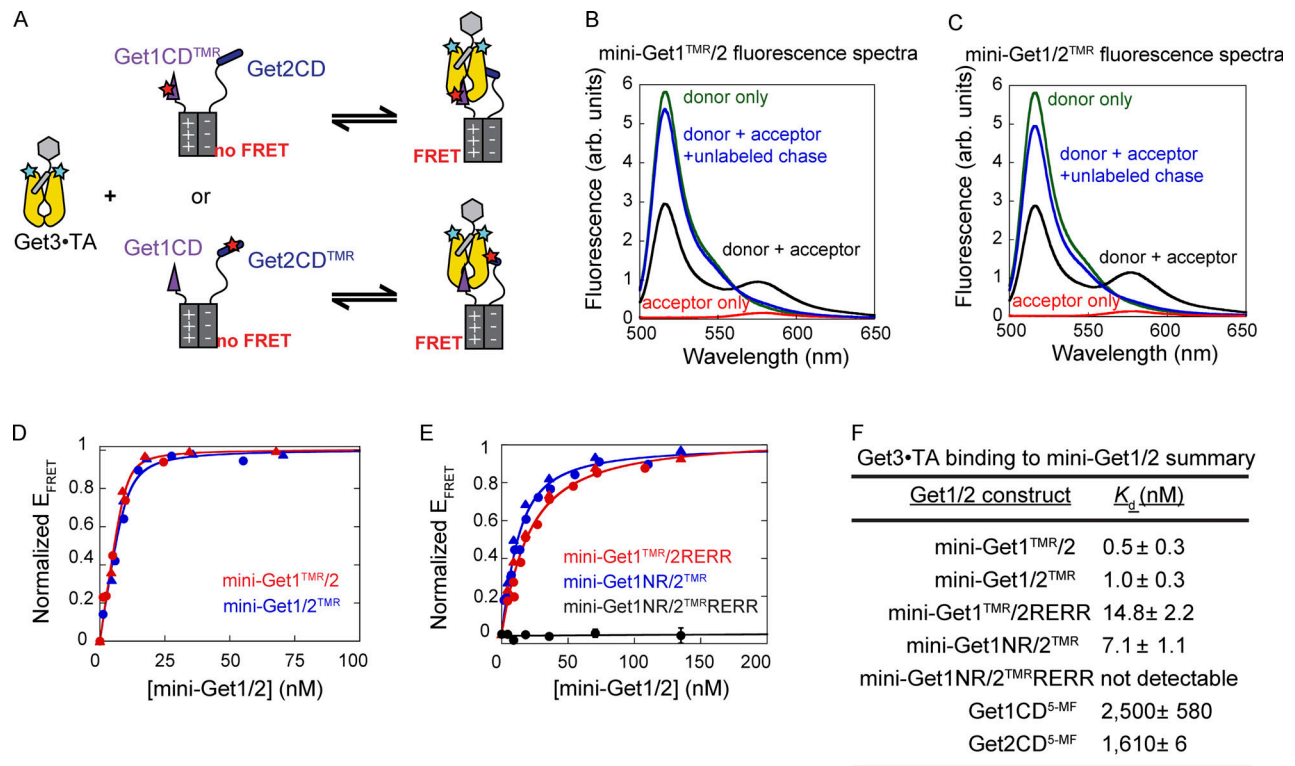
(NR) in Get1CD or the R14E/E15R/R16E/R17E mutation (RERR) in Get2CD that disrupt binding to Get3, suggesting that both subunits contribute to Get3 binding (Wang et al., 2011). To decipher potential subunit cooperation during capture of the Get3 • TA targeting complex, we quantitatively evaluated the contribution of the individual CDs to the binding of Get3 • TA. We assembled Get3 • TA complexes by in vitro translation of Bos1, a model GET substrate, in *Escherichia coli* lysate in the presence of Get3 and affinity-purified Get3 • TA complexes via the 3xStrep-tag on Bos1 (Rao et al., 2016). Get3 • TA complexes generated by this procedure were kinetically stable and highly efficient in TA targeting and insertion into the ER membrane (Chio et al., 2017b; Rao et al., 2016). To quantitatively characterize the interaction of Get3 with Get1/2, we used Förster resonance energy transfer (FRET) between BODIPY-FL (BDP; donor dye) labeled on Get3 (Rao et al., 2016) and tetramethylrhodamine (TMR; acceptor dye) labeled on Get1CD or Get2CD in mini-Get1/2 (Fig. 1 A). Addition of Get3^{BDP} to mini-Get1^{TMR}/2 or mini-Get1/2^{TMR} led to a ∼50% reduction in donor fluorescence and a corresponding increase in acceptor fluorescence (Fig. 1, B and C; green versus black lines). This fluorescence change was competed away by excess unlabeled mini-Get1/2 (Fig. 1, B and C, black versus blue lines), confirming that the observed fluorescence changes arose from FRET between the dye pair upon interaction of mini-Get1/2 with Get3 • TA.

Equilibrium titrations using this FRET assay showed that mini-Get1/2 binds Get3 • TA tightly, with an equilibrium dissociation constant (K_d) of 0.5–1 nM (Fig. 1, D and F). Similar K_d values were observed regardless of whether Get1CD or Get2CD was labeled, indicating that the tight binding was unlikely to arise from artifacts of fluorescence labeling. To evaluate the contribution of the individual subunits to Get3 • TA binding, we introduced the NR mutation in Get1CD or the RERR mutation in Get2CD. Each mutation weakened the binding of mini-Get1/2 to Get3 • TA 10–30-fold (Fig. 1, E and F). Introduction of both mutations abolished the binding of mini-Get1/2 to Get3 • TA (Fig. 1, E and F), ruling out the possibility that the individual mutations did not completely disrupt the Get3 interaction of the respective CDs, or that artificial stabilizing interactions were introduced by fluorescence labeling.

While the observed mutational effects are consistent with the model that Get1CD and Get2CD co-bind Get3 in the Get1/2 complex (Stefer et al., 2011; Zalisko et al., 2017; Wang et al., 2011), mutants mini-Get1(NR)/2^{TMR} and mini-Get1^{TMR}/2(RERR) retained high affinities for Get3 • TA, with K_d values of 7.1 nM and 14.8 nM, respectively (Fig. 1 F). These affinities are ∼220- and ∼170-fold higher than those measured previously with isolated Get2CD and Get1CD, respectively (Fig. 1 F; Rome et al., 2014). These results suggest that, in addition to avidity effects, the assembly of Get1CD with Get2CD in mini-GET1/2 induced conformational changes in the CDs that greatly enhanced their individual affinities for the Get3 • TA complex.

Both Get1CD and Get2CD are required for efficient Get3•TA disassembly

We next determined the contributions of the individual Get1/2 subunits to disassembly of the Get3 • TA complex. To this end,

Chio et al.
Receptor subunit cooperation drives TA targeting

Journal of Cell Biology   2 of 16
https://doi.org/10.1083/jcb.202103079

Figure 1. Assembly of the Get1 and Get2 CDs enhances the binding affinity of the individual subunits for Get3•TA. (A) Scheme of the FRET assay to measure the binding of Get3•TA to mini-Get1/2. Get3 was labeled with BDP (donor dye; cyan stars), and mini-Get1/2 was labeled with TMR on Get1CD or Get2CD (acceptor dye; red star). **(B)** Fluorescence emission spectra of the following Get3•mini-Get1/2 complexes upon excitation of the donor dye: (1) Get3^{BDP} with unlabeled mini-Get1/2 (green); (2) Get3^{BDP} with mini-Get1/2 labeled with TMR on Get1CD (mini-Get1^{TMR}/2; black); (3) sample (2) chased with 1 µM unlabeled mini-Get1/2 (blue); and (4) unlabeled Get3 with mini-Get1^{TMR}/2 (red). Reactions contained 20 nM Get3^{BDP} and 10 nM mini-Get1^{TMR}/2 where indicated. **(C)** Same as in B, except that the TMR dye was labeled on Get2CD (mini-Get1/2^{TMR}). **(D and E)** Equilibrium titrations to measure the binding of Get3^{BDP}•TA to mini-Get1^{TMR}/2 (red) and mini-Get1/2^{TMR} (blue; D), and to mutants mini-Get1^{TMR}/2(RERR) (red), mini-Get1(NR)/2^{TMR} (blue), and mini-Get1(NR)/2^{TMR}(RERR) (black; E). Solid circles and triangles indicate the data from independent titrations. Observed FRET values were normalized and fit to Eq. 2 in Materials and methods, and the obtained K_d values are reported in F. For mini-Get1(NR)/2^{TMR}(RERR) (black), error bars denote SD of the measurements, with n = 2. **(F)** Summary of the K_ds of Get3•TA for WT and mutant mini-Get1/2 complexes. The previously reported K_d values of Get3•TA for the individual Get1 and Get2 CDs labeled with fluorescein-5-maleimide (5-MF) are shown for comparison (Rome et al., 2014). Values are reported as optimized value ± square root of covariance (a measure of fitting error).

we used a previously developed FRET assay based on a donor dye, coumarin (Cm), labeled on the TA-TMD, and an acceptor dye, BDP, labeled on Get3 (Rao et al., 2016). TA dissociation from Get3 was induced by chasing a preassembled Get3^{BDP}•TA^{Cm} complex (15 nM) with an excess amount (20 µM) of a plant-derived membrane protein chaperone, which traps any dissociated TAs (Fig. 2 A, TA trap). The dissociation kinetics was determined by real-time measurement of the recovery of donor (Cm) fluorescence due to FRET loss between dyes. In the absence of mini-Get1/2, the Get3•TA complex dissociated slowly, with a $t_{1/2}$ of ~160 min (TA-trap only in Fig. 2 C and Chio et al., 2019). The additional presence of mini-Get1/2 accelerated TA release from Get3 fivefold to sixfold (Fig. 2, B and C; $t_{1/2}$ ~30 min). The Get1(NR) or Get2(RERR) mutation each reduced the rate of TA release from Get3 (Fig. 2, B and C; $t_{1/2}$ ~60 min), and introduction of both mutations resulted in a TA release rate similar to spontaneous Get3•TA dissociation (Fig. 2, B and C; $t_{1/2}$ ~180 min). These experiments were performed at mini-Get1/2 concentrations (3 µM) far above their respective K_ds for Get3•TA (Fig. 1 F); thus, the observed defects of mini-Get1(NR)/2 and

mini-Get1/2(RERR) in TA release could not be attributed to incomplete Get3•TA binding. These results suggest that both the Get1 and Get2 CDs play direct roles in the disassembly of Get3•TA complexes, and argue against models in which Get1CD is solely responsible for triggering TA release from Get3 (Mariappan et al., 2011; Stefer et al., 2011; Wang et al., 2011).

Get2CD induces Get3 opening

The observation that mini-Get1(NR)/2 significantly accelerated Get3•TA disassembly (Fig. 2) strongly suggests that Get2CD can also remodel Get3•TA to facilitate TA release. To directly test this hypothesis, we used an established solution-based smFRET assay that monitors the global conformation of individual Get3 dimers at equilibrium (Chio et al., 2017b). In this assay, Get3 dimers are doubly labeled with donor and acceptor fluorophores such that *closed* Get3 displays high FRET, whereas *open* Get3 displays low FRET (Fig. 3 A; and Fig. S2, A and B). Both the stoichiometry (S) and effective FRET efficiency (E*) of individual Get3 dimers can be detected and quantified as they diffuse through a femtoliter-scale observation volume, using confocal
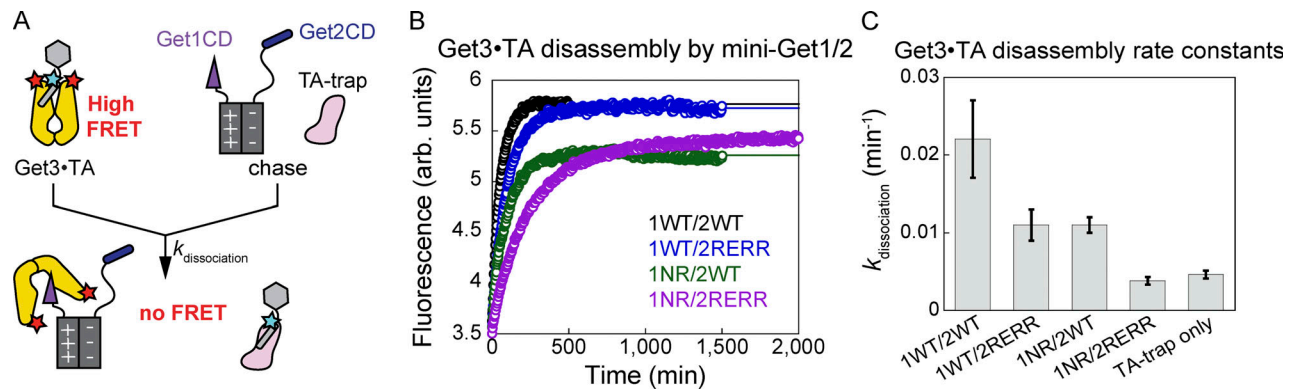
Figure 2. Get1 and Get2 CDs cooperate for efficient Get3•TA disassembly. (A) Scheme of the FRET assay to measure Get3•TA disassembly. Purified Get3•TA complexes contain 7-hydroxycoumarin (Cm; donor dye; cyan star) labeled on the TA-TMD and BDP (acceptor dye; red stars) labeled on Get3, which gives efficient FRET between the dye pair. Dissociation of TA from Get3 was initiated by addition of the TA trap with and without mini-Get1/2 and results in loss of FRET. **(B)** Time courses of Get3•TA disassembly in the presence of WT mini-Get1/2 (black), mini-Get1/2(RERR) (blue), mini-Get1(NR)/2 (green), and mini-Get1(NR)/2(RERR) (purple). 15 nM Get3•TA was chased with 3 µM of the indicated mini-Get1/2 complexes and 20 µM TA-trap in each reaction, and the changes in donor fluorescence intensity were recorded in time. **(C)** Summary of the Get3•TA disassembly rate constants in the absence and presence of the WT and mutant mini-Get1/2 complexes. Data are reported as mean ± SD, with n = 3.

microscopy with alternating laser excitation with microsecond time resolution (µs-ALEX; Kapanidis et al., 2005). To better resolve the *open* conformations, we used a FRET pair with a longer Förster radius (ATTO 550/ATTO 647N; R_0 ~65 Å) than the Cy3B/ATTO 647N pair used in the previous study (Chio et al., 2017b). Analysis on Get3 labeled with only the donor or acceptor dye showed that Get1CD and Get2CD do not alter the dye photophysics in a manner that will alter the observed FRET efficiency (Fig. S2 C). Therefore, the observed changes in FRET efficiency can be attributed to global conformational changes in Get3.

Apo-Get3 displayed a broad smFRET histogram that peaked at E* values of ~0.7–0.9 (Fig. 3 B, black outline), as reported previously (Chio et al., 2017b). Addition of Get2CD shifted the FRET histogram of Get3 toward lower FRET efficiencies, with a new peak at E* ~0.4 (Fig. 3 B, gray bars versus black outline), indicating that Get2CD induced Get3 *opening*. As predicted from previous structural and biochemical data (Kubota et al., 2012; Mariappan et al., 2011; Stefer et al., 2011), Get1CD induced extensive *opening* of Get3, such that the FRET histogram is dominated by a peak at E* ~0.3 (Fig. 3 B, magenta outline). In addition to apo-Get3, Get2CD also induced Get3 *opening* in the presence of ADP (Fig. 3 C), but not in the presence of ATP (Fig. 3 D). The same results were observed using Get3 labeled with the Cy3B/ATTO 647N FRET pair, except that the FRET histograms are shifted toward lower E* values due to the shorter Förster radius of this dye pair (Fig. S2, D–G). Together, these results provide direct evidence that, in addition to Get1CD, Get2CD can also remodel Get3 and bias its conformation to more *open* states.

To better mimic the in vivo function of Get1/2, we tested how mini-Get1/2 regulates the conformation of the Get3•TA complex. The smFRET histogram of Get3•TA displays a major peak at E* ~0.9, with a highly populated tail extending toward lower FRET values (Fig. 4, A and E). This confirms the results of previous work showing that the TA substrate induces Get3 to sample open conformations (Chio et al., 2017b). Addition of

mini-Get1/2 shifted the smFRET histogram of Get3•TA to lower FRET values, with a major peak at E* ~0.35 and a minor peak at E* ~0.9 (Fig. 4, B and E). In comparison, the low FRET population was more dominant with mini-Get1/2(RERR) bound to Get3•TA (Fig. 4, C and E), consistent with previous crystallographic results showing that Get1CD induces a highly *open* Get3 (Kubota et al., 2012; Mariappan et al., 2011; Stefer et al., 2011). Mini-Get1(NR)/2 also shifted the smFRET histogram, reducing the peak at E* ~0.9 and inducing a new peak at E* ~0.35 (Fig. 4, D and E), although the low FRET state was less populated compared to that with WT mini-Get1/2 (Fig. 4, A and E). Thus, Get2CD also induces *opening* of Get3•TA, but less extensively compared with Get1CD.

To further determine whether the conformational heterogeneity of Get3•TA is dynamic or static in nature, we implemented burst variance analysis (BVA), which detects dynamic conformational sampling by comparing the SD of E* over time with the SD expected from shot noise (Fig. S2, H–K). If multiple conformations interconvert on the sub-millisecond or faster timescale, the SD of sub-bursts in each burst would be higher than the expected shot noise–limited SD (static limit; Fig. S2, H–K, red lines; Torella et al., 2011). Get3•TA exhibiting intermediate E* values (0.5–0.7) displayed higher SD than the static limit (Fig. S2 H), consistent with our previous report (Chio et al., 2017b). This indicates that TA-bound Get3 dynamically samples *open* conformations and that the observed intermediate E* values are due to averaging of Get3•TA complexes in lower and higher FRET states that interconvert on the sub-millisecond or faster timescale. Get3•TA remains highly dynamic when bound to all the mini-Get1/2 constructs, transitioning between low and high FRET states on the sub-millisecond timescale (Fig. S2, I–K).

Notably, mini-Get1/2(RERR) is less efficient than mini-Get1/2 in facilitating TA release from Get3 (Fig. 2, B and C) despite its ability to induce a more open Get3 (Fig. 4, C and E). This provides additional evidence that the defect of mini-Get1/2(RERR)
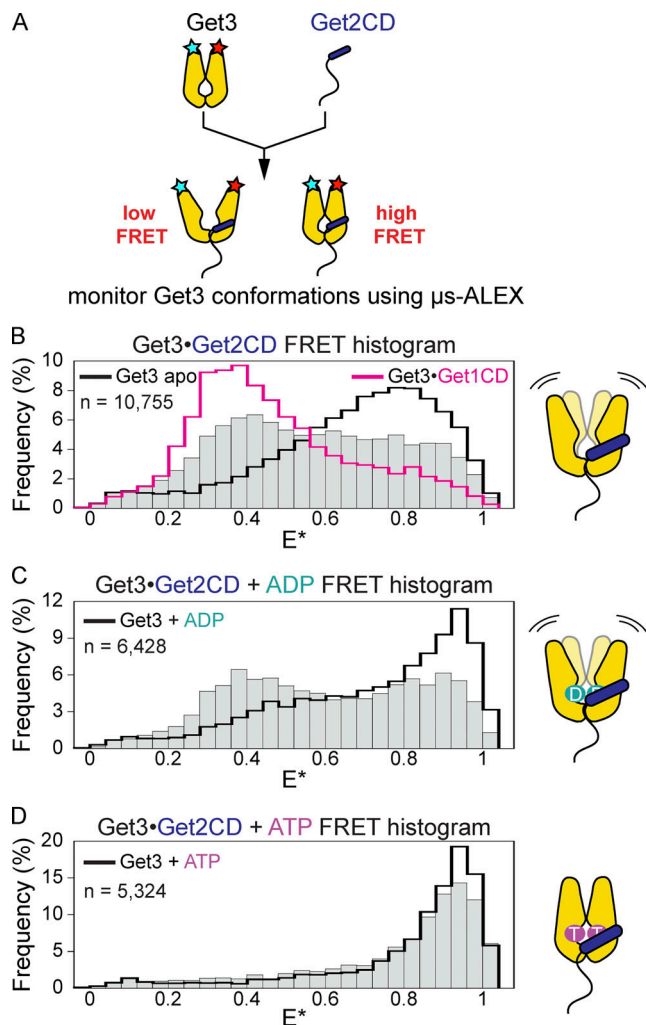
Figure 3. **Get2CD induces Get3 opening. (A)** Schematic of the smFRET measurements to monitor the global conformational distribution of Get3. Get3 is doubly labeled with ATTO 550 (donor dye; cyan star) and ATTO 647N (acceptor dye, red star), which displays high FRET if Get3 is *closed* and low FRET if Get3 is *open*. **(B–D)** smFRET histograms of Get3 bound to Get2CD (gray bars) in the absence (B) and presence of 2 mM ADP (C) or 2 mM ATP (D). Saturating Get2CD (10 μM) was used in all experiments. The smFRET histograms of apo-Get3 (black outline) and Get3 bound to Get1CD (pink outline) are shown for comparison. "n" denotes the number of bursts used to generate the Get3•Get2CD FRET histogram. The degree of Get3 opening (Ratio$^{open/closed}$) is semi-quantitatively calculated and presented in Fig. 5 G.

in Get3•TA disassembly cannot be attributed to weaker binding of mini-Get1/2(RERR), and suggests that increased sampling of the *open* conformation does not necessarily lead to more efficient Get3•TA disassembly. Instead, our results suggest that Get1CD and Get2CD together induce an intermediary degree of Get3 *opening*, in which both the *open* and *closed* states are sampled, and that this conformational balance is conducive to trigger the most efficient TA release.

MoRFs in the Get2 linker mediate Get3 remodeling

The ability of Get2CD to induce Get3 opening is unexpected, as the conserved N-terminal helix of Get2CD (residues 1–40) cocrystallized with *closed* Get3 and binds to one of the subunits in
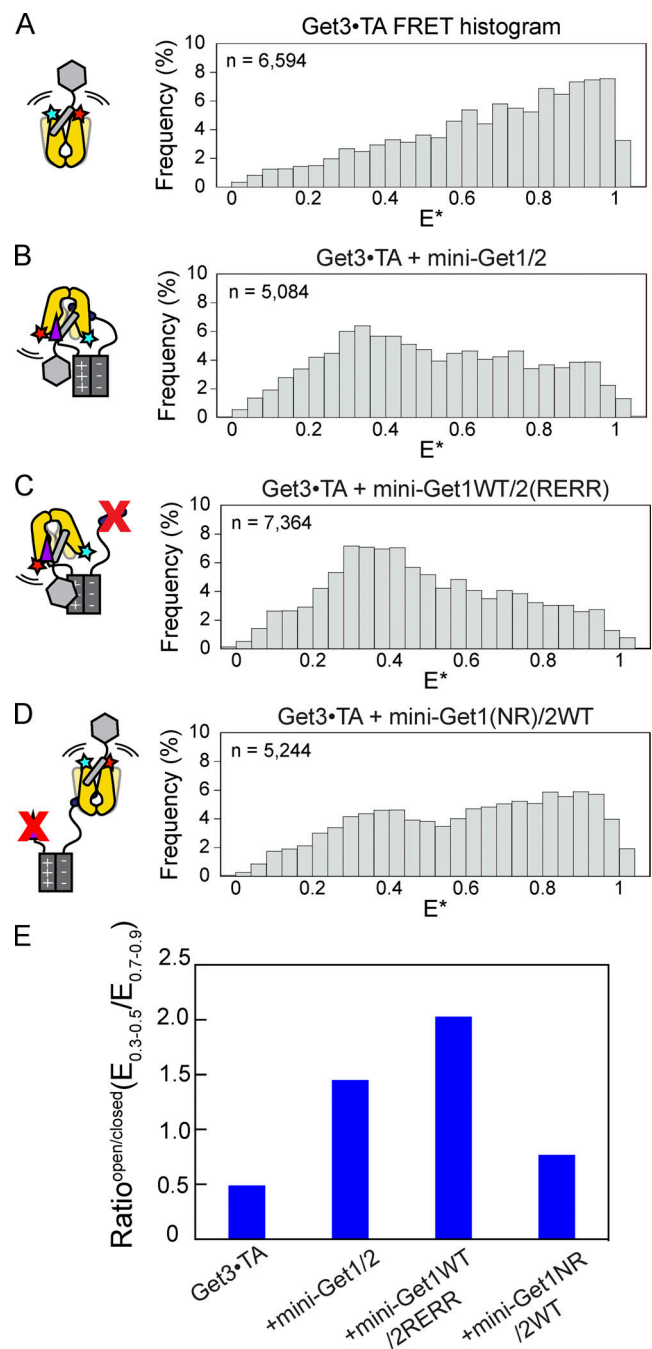
Figure 4. **Get1CD and Get2CD together tune the conformational distribution of Get3•TA. (A–D)** smFRET histograms of Get3•TA in the absence (A) and presence of WT mini-Get1/2 (B), mini-Get1/2(RERR) (C), and mini-Get1(NR)/2 (D). Saturating (3 μM) mini-Get1/2 was used in all experiments. "n" denotes the number of bursts used to generate each FRET histogram. **(E)** Quantification of the smFRET histograms from A–D. The degree of Get1/2 CD–induced Get3 opening (Ratio$^{open/closed}$) is semi-quantitatively calculated from the ratio of Get3 bursts in the low FRET bins (E* = 0.3–0.5) to that in the high FRET bins (E* = 0.7–0.9).

the Get3 dimer, in contrast to Get1CD, which inserts at the dimer interface of *open* Get3 (Stefer et al., 2011; Mariappan et al., 2011). Get2CD also contains an ~110–amino acid disordered linker that connects its N-terminal helix to the TMDs. To test whether the N-terminal helix or the linker of Get2CD is responsible for Get3

opening, we purified Get2CD(1–40; Fig. S1 C) and tested its effect on Get3 conformation. Get2CD(1–40) did not significantly change the smFRET histogram of Get3 in both the apo and ADP states (Fig. 5 A), indicating that the disordered linker in Get2CD is required for remodeling Get3.

To search for sequences in the Get2CD linker required to induce Get3 opening, we generated a set of deletion mutants in which 10–20—amino acid segments in the linker sequence are replaced with (GS)₆ (GS1–GS6; Fig. S1 C and Fig. S3 A). smFRET measurements showed that mutants GS2, GS3, and GS4 displayed substantial defects in the remodeling of Get3, whereas GS1, GS5, and GS6 induced Get3 opening similarly to or slightly more efficiently than WT Get2CD (Figs. 5 G and Fig. S3). These results suggest that residues 60–120 in the Get2CD linker contain potential interaction motifs that mediate the conformational remodeling of Get3.

To identify interaction motifs in the Get2CD linker, we analyzed its sequence using multiple predictors for MoRFs, 10–70-residue segments in intrinsically disordered regions (IDRs) that mediate molecular interactions and undergo disorder-to-order transitions upon partner binding (Mohan et al., 2006; Mészáros et al., 2009; Disfani et al., 2012; Fang et al., 2013; Cumberworth et al., 2013; Fung et al., 2018; Oldfield et al., 2008). Three MoRF predictors, ANCHOR, MoRFpred, and MoRF_CHiBi–Web (Fang et al., 2013; Disfani et al., 2012; Malhis et al., 2016), converged on two predicted MoRFs in the Get2CD linker at residues 76–88 and 103–113 (termed H1 and H2, respectively; Fig. 5, B and C). The location of these MoRFs is consistent with observations with the linker deletion mutants (Fig. 5 G and Fig. S3). In addition, two protein secondary structure prediction programs, PSIPRED (Jones, 1999) and RaptorX (Källberg et al., 2012), predicted high helical propensity in H1 and H2 (Fig. S4, A and B). Finally, H1 and H2 contain multiple residues conserved in their hydrophobic nature despite the overall poor sequence conservation of the Get2CD linker (Notredame et al., 2000; Fig. 5 B and Fig. S4 C).

To test the role of H1 and H2, we replaced the hydrophobic residues in each or both MoRFs with glycine, generating mutants Get2CDΔH1, Get2CDΔH2, and Get2CDΔH1ΔH2 (Fig. 5 B). Get2CDΔH1 and Get2CDΔH2 displayed substantially reduced ability to induce the opening of Get3 in both the apo and ADP states (Fig. 5, D, E, and G), and mutation of both H1 and H2 abolished Get3 opening (Fig. 5, F and G). To test whether these remodeling defects arise from weakened binding of the Get2CD MoRF mutants with Get3, we introduced the ΔH1ΔH2 mutation in mini-Get1/2. Using the FRET assay between Get3^BDP and mini-Get1/2^TMR (Fig. 1 A; and Fig. S2, A and B), equilibrium titrations showed that mini-Get1/2 and mini-Get1(NR)/2 bound Get3 with the same affinity, within error, regardless of the presence of the MoRFs (Fig. 6, A–C and E). This excludes the possibility that the remodeling defects of mutant Get2ΔH1ΔH2 are due to weakened binding. When the RERR motif in Get2 was mutated, though, mutation of H1 and H2 weakened the affinity of mini-Get1^TMR/2(RERR) twofold (Fig. 6, D and E), suggesting that the Get2 MoRFs could facilitate the interaction of the Get1 subunit with Get3. Together, these data indicate that high-affinity binding between Get2CD and Get3 is primarily mediated by the N-terminal helices in Get2, whereas the remodeling of Get3 requires both MoRFs in the disordered Get2CD linker.

A helical wheel analysis further suggested that both MoRFs form amphiphilic helices that present a contiguous hydrophobic surface (Fig. 7 A), through which direct interactions between the disordered Get2CD linker and Get3 could be formed. To test whether H1 and H2 directly interact with Get3 to induce conformational changes, we used amber suppression to incorporate a zero-length photo–cross-linker, Bpa, in the H1 (Ala85) or H2 (Ser111) motifs (Fig. 7 A and Fig. S1 C, H1^Bpa and H2^Bpa). We observed efficient cross-links of Get3 with both Get2CD_H1^Bpa and Get2CD_H2^Bpa that are dependent on UV and the Bpa cross-linker (Fig. 7 B). In addition, mutation of conserved hydrophobic residues in H1 and H2 abolished the cross-link (Fig. 7 C). These results provide strong evidence for direct interactions of H1 and H2 directly contact Get3.

Collectively, the results in this section show that the disordered linker of Get2CD contains two conserved MoRFs, which directly interact with Get3 and are responsible for mediating the conformational remodeling of Get3.

Get2-induced Get3 opening is important for efficient TA insertion in vivo

Finally, we asked whether the ability of Get2CD to mediate Get3 opening is important for TA insertion into the ER in vivo. To this end, we used an established model GET substrate, in which BirA is fused to the C-terminal targeting sequence of the SNARE protein Bos1 (Fig. 8 A, BirA-Bos1) and constitutively expressed from a low copy plasmid in yeast cells (Cho and Shan, 2018). An engineered C-terminal opsin tag allows efficient glycosylation of BirA-Bos1 upon insertion into the ER lumen, providing a quantitative readout for insertion efficiency. To test the role of the Get2 H1 and H2 motifs in TA insertion in vivo, we replaced genomic GET2 in Saccharomyces cerevisiae with GET2-FLAG, get2ΔH1-FLAG, get2ΔH2-FLAG, or get2ΔH1ΔH2-FLAG.

The steady-state insertion efficiency of BirA-Bos1 in yeast cells was unaffected by mutations in the H1 or H2 motifs of Get2 (Fig. S5 A). When the insertion kinetics of newly synthesized TAs was measured using a pulse-chase assay, a modest but reproducible delay in BirA-Bos1 insertion was detected at early time points (1 min) with Get2 mutants bearing the ΔH1 and/or ΔH2 mutation (Fig. 8, B–D; and Fig. S5 B). As controls, we also introduced the NR and RERR mutations into genomic GET1 and GET2, respectively, and verified that both mutations induced a 10–15% reduction in the steady-state TA insertion level and impaired the insertion kinetics of BirA-Bos1 (Fig. 8 B and Fig. S5 B). The delay in TA insertion cannot be explained by lower expression levels of the Get2 mutants compared with WT Get2 (Fig. S5 C). Thus, the H1 and H2 motifs on Get2CD, which specifically mediate Get3 opening, facilitate GET-dependent TA insertion in vivo.

Discussion

To ensure efficient membrane protein biogenesis, receptor and/or translocase complexes at the target membrane must effectively capture the targeting complex in the cytosol and remodel their conformation to induce the release of nascent membrane proteins at the site of their insertion. In this work, biochemical,
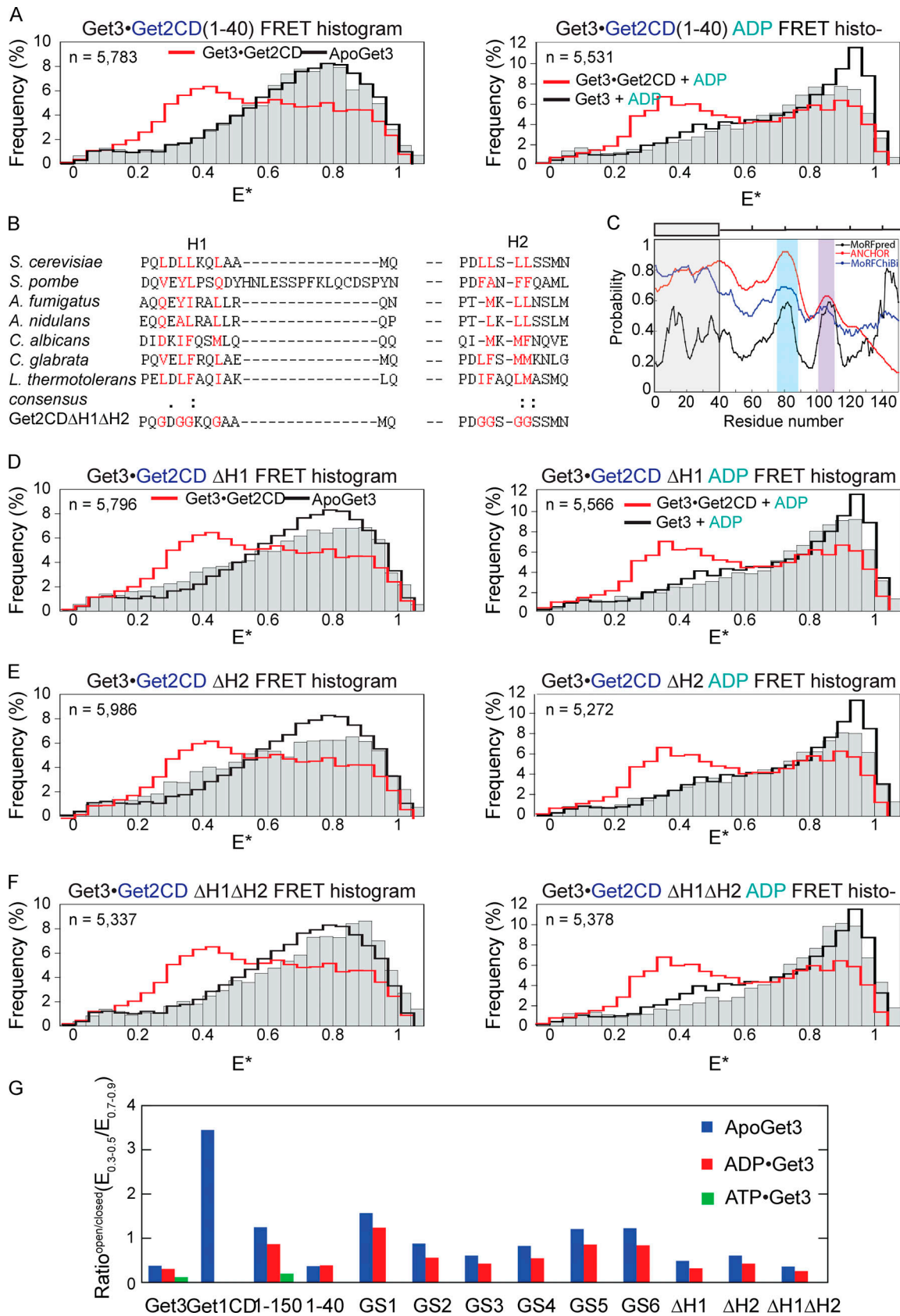
Chio et al.
Receptor subunit cooperation drives TA targeting

Journal of Cell Biology 6 of 16
https://doi.org/10.1083/jcb.202103079

A Get3•Get2CD(1–40) FRET histogram — n = 5,783; Get3•Get2CD (red), ApoGet3 (black)

Get3•Get2CD(1–40) ADP FRET histo- — n = 5,531; Get3•Get2CD + ADP (red), Get3 + ADP (black)

B

	H1		H2
S. cerevisiae	PQLDLLKQLAA---------------MQ	--	PDLLS-LLSSMN
S. pombe	DQVEYLPSQDYHNLESSPFKLQCDSPYN	--	PDFAN-FFQAML
A. fumigatus	AQQEYIRALLR---------------QN	--	PT-MK-LLNSLM
A. nidulans	EQQEALRALLR---------------QP	--	PT-LK-LLSSLM
C. albicans	DIDKIFQSMLQ---------------QQ	--	QI-MK-MFNQVE
C. glabrata	PQVELFRQLAE---------------MQ	--	PDLFS-MMKNLG
L. thermotolerans	PELDLFAQIAK---------------LQ	--	PDIFAQLMASMQ
consensus	. :		::
Get2CDΔH1ΔH2	PQGDGGKQGAA---------------MQ	--	PDGGS-GGSSMN

C MoRFpred (black), ANCHOR (red), MoRFChiBi (blue); Probability vs Residue number

D Get3•Get2CD ΔH1 FRET histogram — n = 5,796; Get3•Get2CD (red), ApoGet3 (black)

Get3•Get2CD ΔH1 ADP FRET histogram — n = 5,566; Get3•Get2CD + ADP (red), Get3 + ADP (black)

E Get3•Get2CD ΔH2 FRET histogram — n = 5,986

Get3•Get2CD ΔH2 ADP FRET histogram — n = 5,272

F Get3•Get2CD ΔH1ΔH2 FRET histogram — n = 5,337

Get3•Get2CD ΔH1ΔH2 ADP FRET histo- — n = 5,378

G $Ratio^{open/closed}(E_{0.3-0.5}/E_{0.7-0.9})$ vs Get3, Get1CD, 1–150, 1–40, GS1, GS2, GS3, GS4, GS5, GS6, ΔH1, ΔH2, ΔH1ΔH2 — ApoGet3 (blue), ADP•Get3 (red), ATP•Get3 (green)

Figure 5. **Two MoRFs in the Get2CD are required for Get3 opening. (A)** smFRET histogram of apo-Get3 (left) and ADP-bound Get3 (right) bound to Get2CD (1–40; gray bars). The smFRET histograms of free Get3 (black outline) and Get3 bound to WT Get2CD (red outline) are shown for comparison. "n" denotes the number of bursts used to generate the smFRET histograms with Get2CD (1–40). **(B)** Sequence alignment of the predicted Get2CD H1(76–88) and H2(103–113)

helices (Fig. S4 C). Conserved hydrophobic residues and their mutations in the ΔH1, ΔH2, and ΔH1ΔH2 mutants are highlighted in red. **(C)** Prediction of MoRFs in GET2CD (1–150) using MoRFpred (Disfani et al., 2012), ANCHOR (Mészáros et al., 2009), and MoRF$_{CHiBi\text{—}Web}$ (Malhis et al., 2016). ScGet2 residues 1–150 were used as the input sequence for all the analysis. The gray bar denotes the N-terminal helices that cocrystalized with Get3 (PDB 3ZS9); the blue and purple columns highlight H1 (residues 76–88) and H2 (residues 103–113), respectively. **(D–F)** smFRET histograms of apo-Get3 (left) and ADP-Get3 (right) bound to mutants Get2CDΔH1 (D), Get2CDΔH2 (E), and Get2CDΔH1ΔH2 (F) are shown as gray bars. The smFRET histograms of free Get3 (black outline) and Get3 bound to WT Get2CD (red outline) in the respective nucleotide states are shown for comparison. "n" denotes the number of bursts used to generate the FRET histogram. **(G)** The degree of Get3 opening (Ratio$^{open/closed}$) is semi-quantitatively calculated from the ratio of Get3 bursts in the low FRET bins (E* = 0.3–0.5) to that in the high FRET bins (E* = 0.7–0.9) for apo-Get3 (blue), ADP•Get3 (red), and ATP•Get3 (green) bound to the indicated Get2CD variants. The ratios for Get1CD-apoGet3, ATP•Get3, and Get2CD-ATP•Get3 were calculated using the smFRET data from Fig. 3, B–D.

biophysical, and sm fluorescence experiments shed light on how the two subunits in the Get1/2 translocase complex coordinate to remodel the Get3 targeting factor for efficient substrate release during the post-translational targeting of tail-anchored membrane proteins to the ER. In contrast to previous models, in which the role of Get2 is restricted to the initial recruitment of Get3 • TA and Get1 is solely responsible for Get3 • TA disassembly (Mariappan et al., 2011; Stefer et al., 2011; Wang et al., 2011), our
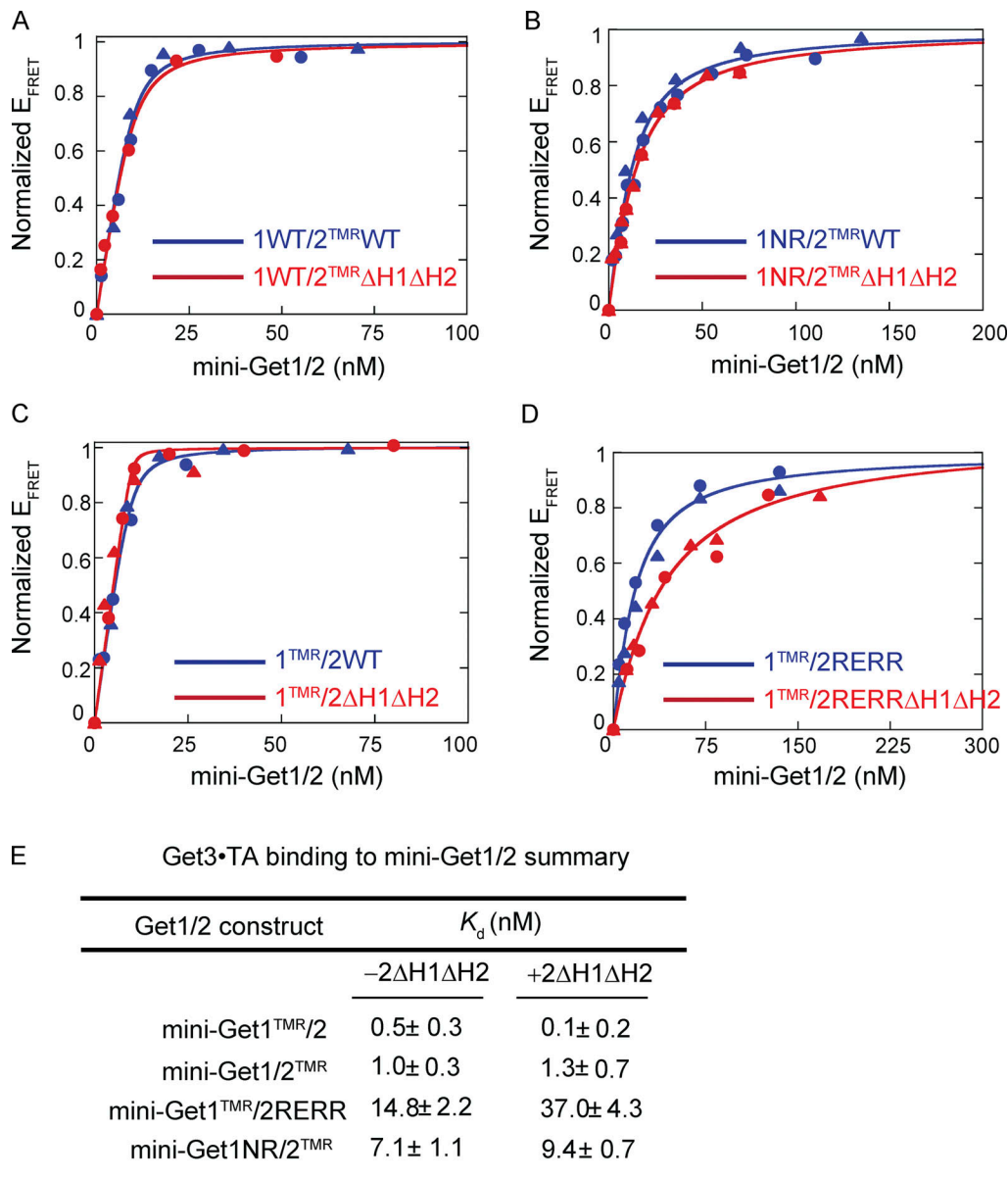

Figure 6. Binding equilibria between mini-Get1/2 variants and the Get3•TA complex. (A–D) Equilibrium titrations to measure the binding of Get3^{BDP}•TA to mini-Get1/2 with the indicated mutations and TMR labeling sites. Data from duplicate measurements are denoted as circles and triangles for each titration. Measured FRET values were normalized and fit to Eq. 2 in the Materials and methods, and the obtained the K_d values are reported in E. **(E)** Values of K_d are reported as optimized value ± square root of covariance (a measure of fitting error).

The table shown in panel E:

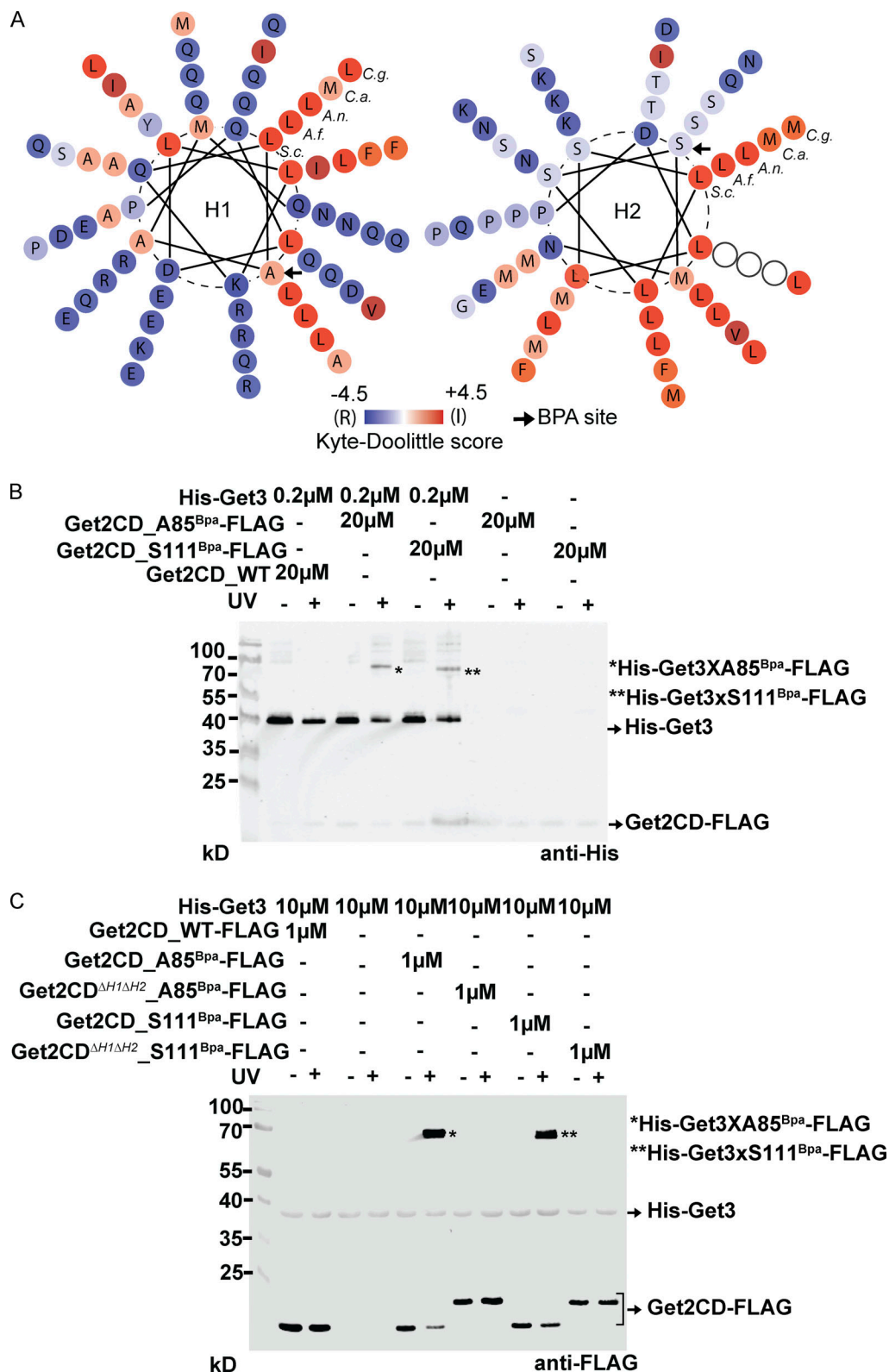| Get1/2 construct	K_d (nM)	
	−2ΔH1ΔH2	+2ΔH1ΔH2
mini-Get1^{TMR}/2	0.5± 0.3	0.1± 0.2
mini-Get1/2^{TMR}	1.0± 0.3	1.3± 0.7
mini-Get1^{TMR}/2RERR	14.8± 2.2	37.0± 4.3
mini-Get1NR/2^{TMR}	7.1± 1.1	9.4± 0.7

Figure 7. **Bpa-mediated photo–cross-linking of the Get2CD H1 and H2 to Get3. (A)** Helical wheel diagrams of the predicted Get2CD H1 and H2 helixes from different species. The diagram was generated in Pepwheel (http://www.bioinformatics.nl/cgi-bin/emboss/pepwheel) with minor modifications on the graphic format. The default *number of steps* and *turns* (18 and 5, respectively) were used as input parameters. Residues are colored in the Kyte and Doolittle hydrophobicity scale (Kyte and Doolittle, 1982). The Bpa incorporation sites of the photo–cross-linker (A85 and S111) are indicated as black arrows. The Get2 sequences analyzed from different species were denoted as S.c. (*S. cerevisiae*), A.f. (*Aspergillus fumigatus*), A.n. (*Aspergillus nidulans*), C.a. (*Candida albicans*), and C.g. (*Candida glabrata*). **(B)** The photo–cross-linker Bpa was incorporated at the indicated residues in H1(A85) and H2(S111) in Get2CD using amber suppression. "*" and "**" denote the cross-linked Get2CDxGet3 complex. WT Get2CD without Bpa was used as a negative control. **(C)** Cross-linking Get2CD^Amb-FLAG was cross-linked with His-Get3 on dry ice for 15 min, and samples were analyzed using the anti-FLAG antibody. "*" and "**" denote the cross-linked Get2CDxGet3 complex. WT Get2CD-FLAG without Bpa was used as a negative control.
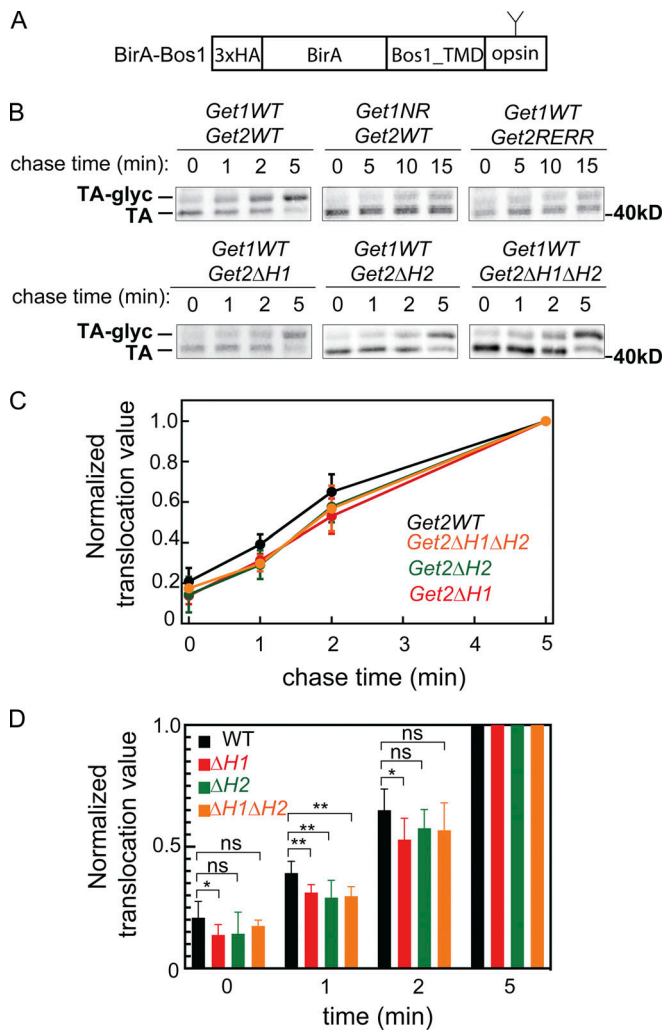
Figure 8. Get2CD linker mutants attenuated TA insertion into the ER in vivo. (A) Schematic of the model TA substrate used for the in vivo insertion assay. BirA-Bos1 contains, from the N to the C terminus, an N-terminal 3xHA tag, the BirA protein, the TMD of Bos1, and an opsin tag that is efficiently glycosylated (glyc) upon insertion into the ER. "Y" depicts the glycosylation site. **(B)** Representative autoradiographs are shown for the pulse-chase assays to measure the kinetics of TA translocation to ER in vivo for yeast strains with different Get2 variants as indicated. The complete set of replicates is shown in Fig. S5 B. **(C)** Quantification of the data from B and additional biological replicates in Fig. S5 B. The steady-state TA translocation levels are the same among yeast strains with different Get2 variants (Fig. S5 A). Hence, all the TA translocation values were normalized to the end point. Error bars denote SD, with n = 5–8 biological replicates. **(D)** Statistical analysis on the difference between WT and each Get2 variant using an unpaired two-sided t test (assuming that both populations have the same SD and follow Gaussian distribution). The P values for each significant different ($P \leq 0.05$) pair are $P^{0min}_{WT/H1}$ = 0.0332; $P^{1min}_{WT/\Delta H1}$ = 0.0028; $P^{1min}_{WT/\Delta H2}$ = 0.0083; $P^{1min}_{WT/\Delta H1\Delta H2}$ = 0.0036; and $P^{2min}_{WT/\Delta H1}$ = 0.0192. *, $P \leq 0.05$; **, $P \leq 0.01$.

results uncover a new role of Get2 in regulating the conformation of Get3 and reveal extensive cooperation between the Get1 and Get2 subunits during the capture and remodeling of Get3•TA. These results identify a previously unappreciated and mechanistically important step in the membrane-associated events in the GET pathway and, together with other works, emphasize the role of IDRs in the function of receptor and translocase complexes during protein biogenesis.

Previous measurements using isolated CDs reported low binding affinities of Get1CD and Get2CD for the Get3•TA complex, with K_ds in the micromolar range (Rome et al., 2014). Coupled with the low in vivo concentration of Get1/2, this posed questions as to how the targeting complex is efficiently captured at the ER membrane. The measurements here show that, when assembled into the mini-Get1/2 complex, the individual Get1CD and Get2CD subunits display low nanomolar affinities for Get3•TA, two orders of magnitude higher than the affinities observed with the isolated CDs (Fig. 1 F; Rome et al., 2014). The precise mechanism underlying this affinity enhancement remains to be determined, but a few models can be excluded based on available data. The enhanced binding is unlikely to be due to a Get1- or Get2-induced conformational change of Get3, as high-affinity binding was still observed even when the Get3 binding site in the other subunit was mutated (Fig. 1 F, compare the K_d of mini-Get1[NR]/2^{TMR} versus Get2CD, or the K_d of mini-Get1^{TMR}/2[RERR] versus Get1CD). The enhanced binding is also unlikely to arise from oligomerization of mini-Get1/2. Size-exclusion chromatography coupled with multi-angle light scattering (SEC-MALS) measurements showed that mini-Get1/2 is a heterodimer (Fig. S1 B), as expected. Although a recent work strongly suggests that Get3 induces Get1/2 tetramerization (McDowell et al., 2020), tetramer formation is mediated by the Get1/2 TMDs and is unlikely to occur with mini-Get1/2. The absence of cooperativity during the binding of mini-Get1/2 to Get3•TA (Fig. 1) also provided no indication of Get3-induced oligomerization of mini-Get1/2. While Get1CD and Get2CD do not appear to display significant interactions with one another (Zalisko et al., 2017), it is possible that transient interactions occur between the Get1 and Get2 CDs when they are positioned in close proximity in a complex, which primes their conformations for more favorable Get3•TA interaction.

Although previous biochemical and crystallographic studies found no evidence for a role of Get2CD in regulating the conformation of Get3 (Mariappan et al., 2011; Stefer et al., 2011), the smFRET measurements directly visualized Get3 *opening* by Get2CD (Fig. 3). Consistent with previous observations in crystallographic analyses, the highly conserved N-terminal helices of Get2CD that bind Get3 (Stefer et al., 2011; Mariappan et al., 2011) do not contribute to the remodeling of Get3 (Fig. 5 A). In contrast, the intrinsically disordered linker in Get2, which connects the N-terminal helices to its TMDs, contains two semi-conserved MoRF elements, H1 and H2, that are responsible for mediating Get3 opening. MoRFs are elements embedded within the IDRs of a protein that undergo disorder-to-order transitions upon binding with interaction partners (Malhis and Gsponer, 2015; Malhis et al., 2016). The role of H1 and H2 as MoRFs is supported by the conservation of multiple hydrophobic residues that could provide protein interaction sites and by secondary structure analyses that predicted the formation of amphiphilic helices in H1 and H2 (Figs. 5, 7, and S4). The photo–cross-linking of Get3 to Bpa probes engineered in H1 and H2 provided further evidence for direct contacts of these MoRFs with Get3. Although the precise interaction sites of H1/H2 on Get3 remain to be determined, an intriguing possibility is that the hydrophobic face of the H1/H2 helices could invade the TMD binding groove of Get3 to open Get3 and displace the bound TA.

Introduction of the ΔH1ΔH2 mutations did not substantially affect the affinity of mini-Get1/2 for Get3•TA. This indicates that the N-terminal helices of Get2 provide the anchoring contact that enables high-affinity binding of Get2 with Get3•TA, whereas the H1 and H2 MoRFs mediate transient interactions that do not contribute to equilibrium stability. The transient interaction of the Get2 MoRFs with Get3 may also explain the dynamic sampling of Get3 between *open* and *closed* conformations when bound to Get2CD and mini-Get1(NR)/2. When the Get3 interaction sites in the N-terminal helices of Get2 are removed in mini-Get1/2(RERR), however, the additional ΔH1ΔH2 mutations in Get2 modestly weakened the binding affinity to Get3, suggesting an ancillary role of H1 and H2 in assisting the interaction of Get1 with Get3. In the context of the Get1/2 complex at the ER, the additional interaction of the Get2 H1/H2 motifs with Get3•TA could bring the targeting complex closer to the membrane-proximal Get1CD and help initiate the interaction with and further remodeling of Get3 by Get1.

The combined effects of Get1CD and Get2CD in mini-Get1/2 generate a broad conformational landscape for Get3•TA, wherein both the *open* and *closed* conformations are sampled (Fig. 4). Unexpectedly, although the *open* state is more dominant in the mini-Get1/2(RERR)–bound Get3•TA complex (Fig. 4), TA release from this complex is significantly slower compared with that for mini-Get1/2–bound Get3•TA (Fig. 2). As mini-Get1/2 (RERR) binds Get3•TA with a K_d value of 14.8 nM, the lower efficiency of Get3•TA disassembly cannot be attributed to incomplete binding. These results indicate that the Get1-induced opening of Get3•TA is necessary but not sufficient for optimal Get3•TA disassembly. It is plausible that the dynamic sampling of Get3 over a broad conformational landscape is important for optimal TA release. Alternatively or in addition, the hydrophobic face of the H1/H2 helices in Get2 could invade the TMD binding groove of Get3 and help displace the bound TA, as discussed earlier. The observed Get3•TA disassembly rate of ∼0.022 min⁻¹ by mini-Get1/2 is still slower than the rates of TA insertion into yeast rough microsomes from Get3•TA (0.045–0.14 min⁻¹; Rao et al., 2016), strongly suggesting that the TMDs of Get1/2 coordinate with the CDs to provide a more facile conduit for TA release compared with the external TA trap used here. Notably, mutations of H1 and/or H2 delayed TA insertion into the ER in vivo (Fig. 8, 1 min). These effects, though modest, support a role of the MoRFs in the optimal functioning of the Get1/2 receptor in vivo.

Our findings adds a mechanistically important new step for the membrane-associated molecular events in the GET pathway (Fig. 9). After ATP hydrolysis, the Get3•TA complex in the cytosol is initially captured by the N-terminal helices of Get2 (step 1). Get2 forms additional interactions with Get3•TA via the H1 and H2 MoRFs, which initiates the opening of Get3 and brings the targeting complex closer to the ER membrane and to Get1CD (step 2). The interaction of Get1CD with Get3•TA induces further opening of Get3, which together with the Get2 H1 and H2 MoRFs generates a conformational distribution of Get3 (step 3) that is optimal for triggering the release of TA and its subsequent insertion into the lipid bilayer (step 4).

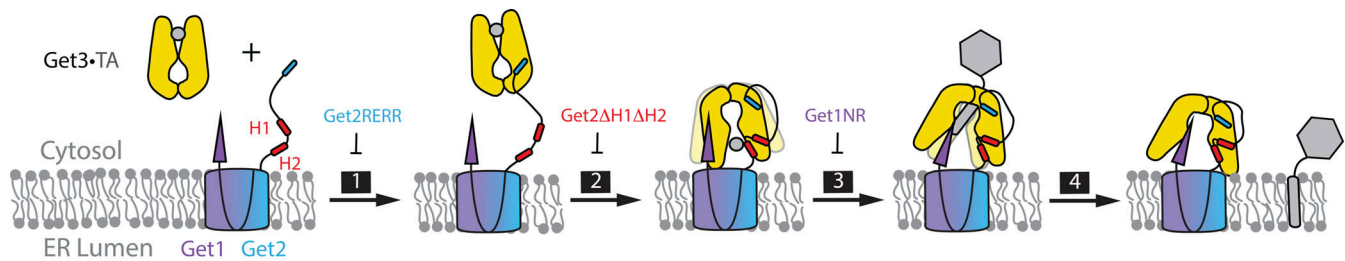Emerging data highlight key roles of IDRs in the function of receptors and translocase complexes during membrane protein biogenesis. Get1/2 and its mammalian homologue, WRB/CAML, share structural homology with the insertase YidC (McDowell et al., 2020), a member of the Alb3/Oxa1/YidC membrane protein insertase family. Oxa1 and YidC use positively charged residues in their disordered C-terminal CDs to mediate interaction with ribosomes during cotranslational targeting (Geng et al., 2015; Jia et al., 2003; Szyrach et al., 2003). The disordered C-terminal domain of Alb3 contains multiple conserved motifs rich in basic residues, which mediate the recruitment and remodeling of the chaperone cpSRP43 to facilitate posttranslational membrane protein insertion into the chloroplast thylakoid membrane (Falk et al., 2010; Liang et al., 2016). Analogously, this and previous work identified multiple protein interaction motifs in the disordered Get2CD of the Get1/2 complex that play crucial roles in recruiting and remodeling the targeting factor Get3 during TA insertion (Mariappan et al., 2011; Stefer et al., 2011). A recent study identified a MoRF in the disordered linker of the mammalian SRP receptor, which plays an essential role in the ribosome-induced SRP receptor assembly during cotranslational protein targeting (Hwang Fu et al., 2019). In general, MoRF elements within IDRs can provide binding sites through transient interactions with binding partners to mediate dynamic cellular processes, such as signaling and complex assembly (van der Lee et al., 2014). The dynamic nature of IDRs also allows MoRFs to recruit binding partners over a longer radius than structured protein domains with the same amino acid length. Our work here further uncovered a new role of MoRFs in the conformational remodeling of protein complexes, which could be envisioned in a variety of protein translocation pathways. As such, interaction motifs embedded within IDRs could serve as interaction hubs to aid in the function of a broad spectrum of receptors and translocase complexes.

Materials and methods

S. cerevisiae strain construction
CRISPR/Cas9-mediated genome editing was used to mutate genomic *GET1* and *GET2* in the BY4741 strain to generate strains harboring *GET2FLAG*, *get2^RERR^FLAG*, *get1^NR^GET2FLAG*, *get2^ΔH1^FLAG*, *get2^ΔH2^FLAG*, and *get2^ΔH1ΔH2^FLAG* (Ryan et al., 2016). Genomic *GET2* was first replaced by *URA3* by cotransforming 1 µg pCAS plasmid encoding *Streptococcus pyogenes* Cas9, an sgRNA with a guide sequence (5′-CAAATGACTGCTTGCCTGCC-3′) that targets the codon for *GET2*(Q36), and 5 µg double-stranded linear repair DNA encoding *URA3* flanked with sequences from *GET2* (5′-CCATGTTTGTAGCATCAGCAACGTAGCTCTAGGAAATAT GTC-3′ and 5′-AAATTCTAGATAGTTCAGTAATATAATACATTG TT-3′). Cells were selected on synthetic defined (SD)-uracil (URA)+G418 (200 mg/l) agar plates. The second round of CRISPR-Cas9 editing replaces *URA3* (pCAS URA3) with *GET2-FLAG* or its mutants using a double-stranded repair DNA fragment that encodes the desired Get2 variant and is flanked by sequences 400 bp upstream and 250 bp downstream of genomic *GET2*. Positive colonies were doubly selected by growth on SD media and no growth on SD-URA media during the second round of CRISPR editing. The final strains were verified by sequencing.

Chio et al.
Receptor subunit cooperation drives TA targeting

Journal of Cell Biology 11 of 16
https://doi.org/10.1083/jcb.202103079

Figure 9. **Revised model for Get1/2-mediated Get3•TA disassembly at the ER.** The Get3•TA complex is captured by the N-terminal helix of Get2CD in the Get1/2 complex (step 1). Get2 forms additional interactions with Get3•TA via the H1 and H2 motifs in its linker, which brings the targeting complex closer to Get1CD and initiates the opening of Get3 (step 2). Get1CD further interacts with Get3•TA and induces additional opening of Get3, generating a conformational distribution that is optimal for TA release (step 3) and insertion into the ER (step 4). The Get2 binding mutant, Get2(RERR), inhibits step 1, Get2ΔH1ΔH2 inhibits step 2, and Get1(NR) inhibits step 3.

Generation and purification of proteins and complexes

Get3, Get1CD, Get2CD, intein-cpSRP43, and their variants were expressed and purified as previously described (Rome et al., 2014; Liang et al., 2016) with slight modifications. In brief, Get3 or its variants were fused to a N-terminal His-SUMO tag. The fusion protein was expressed in *E. coli* BL21 Star (DE3) cells and purified through Ni Sepharose High Performance (GE Healthcare) affinity chromatography followed by the His_6-SUMO protease digestion to remove the His_6-SUMO tag. The untagged Get3 was further purified through gel filtration using a Superdex 200 10/300 GL (GE Healthcare) and buffer exchanged into GET storage buffer (50 mM K-Hepes, pH 7.4, 150 mM KOAc, 5 mM Mg[OAc]$_2$, 20% glycerol, and 2 mM β-mercaptoethanol). Get1CD and Get2CD and their variants were fused to a N-terminal His_6 tag followed by a PreScission protease cut site. His_6-PreScission-Get1CD and His_6-PreScission-Get2CD were purified through nickel-coupled nitrilotriacetic acid (Ni-NTA; GoldBio) affinity chromatography followed by His_6-PreScission protease (a gift of André Hoelz, California Institute of Technology, Pasadena, CA) digestion to remove the His_6 tag. His_6-PreScission protease was further removed by Ni affinity chromatography. The untagged protein was further dialyzed against the GET storage buffer. His_6-cpSRP43 was purified through Ni affinity chromatography followed by anion exchange using a MonoQ 10/100 GL column. The protein was then dialyzed against storage buffer (50 mM K-Hepes, pH 7.4, 200 mM NaCl, and 20% glycerol). T7 RNA polymerase was fused to an N-terminal His_6-PreScission tag. After Ni affinity chromatography, the His_6 tag was removed by PreScission protease, and the untagged T7 RNA polymerase was further purified using a Superdex 200 10/300 GL column (GE Healthcare) and buffer exchanged into the storage buffer (50 mM K-Hepes, pH 7.4, 200 mM NaCl, and 20% glycerol). The purified T7 RNA polymerase was supplemented with 50% glycerol and stored at –30°C. Cm-tRNA synthetase (CmRS) was fused to an N-terminal His_6-tag followed by a PreScission protease cut site (Rao et al., 2016). His_6-PreScission-CmRS was first purified using Ni Sepharose High Performance (GE Healthcare) chromatography, and then the His_6-tag was removed using His_6-PreScission protease. The reaction was next passed through Ni Sepharose High Performance to remove the His_6-PreScission protease and undigested CmRS. Purified CmRS was dialyzed into buffer (50 mM K-Hepes, pH 7.4, 200 mM NaCl, and 20%

glycerol), supplemented with 50% glycerol and stored at –30°C. Sfp phosphopantetheinyl transferase (Sfp) was fused to a C-terminal His_6-tag (Yin et al., 2006). Sfp-His_6 was first purified using Ni-NTA (Qiagen), and then the elution was dialyzed against storage buffer (10 mM Tris-HCl, pH 7.5, 1 mM EDTA, and 10% glycerol).

Mini-Get1/2 was coexpressed using the pETDuet-1 vector (kind gift from Vladimir Denic, Harvard University, Cambridge, MA) as previously described. Briefly, Get1CD(20–102) and Get2CD(1–150) were fused to the engineered C-terminal sequence deriving from pActPL-Gal4AD (Addgene plasmid #15303; EE12RR345L) and pActPL-Gal4DBD (Addgene plasmid #15304; RR12EE345L) that form a stable cc structure (Moll et al., 2001; Wang et al., 2011; Luan et al., 2006). Get1CD contains a His_6 tag at its extreme C terminus that allows for affinity purification, while Get2CD-cc is untagged and was copurified by forming a heterodimer with Get1CD-cc. Mini-Get1/2 was purified using Ni Sepharose High Performance resin (Ni-HP; Cytiva) followed by size exclusion chromatography on a Superdex 75 10/300 GL (GE Healthcare) in GET storage buffer.

The photo–cross-linker p-benzoylphenylalanine (Bpa) was incorporated into residue 85 or 111 in Get2 using amber suppression (Young et al., 2010). The plasmid pEVOL-BpaRS/tRNA$_{CUA}$^{Opt}, which encodes for optimized amber suppressor tRNA (tRNA$_{CUA}$^{Opt}) and evolved tRNA synthetase for Bpa (BpaRS), was cotransformed with pET33b-Get2CD^{Amb}-FLAG-PreScission-His_6 into BL21 Star (DE3) cells (Thermo Fisher Scientific). Cells were grown in LB Miller media at 37°C to OD$_{600}$ of 0.4, at which expression of tRNA$_{CUA}$^{Opt} and BpaRS was induced by addition of 0.2% arabinose and 1 mM Bpa. The expression of Get2CD^{Amb}-FLAG-PreScission-His_6 was induced at OD$_{600}$ of 0.6 with 0.1 mM IPTG, and cell growth was continued for 90 min before harvesting. Full-length Get2CD^{Bpa}-FLAG-PreScission-His_6 was purified using Ni-NTA affinity chromatography. The elution was mixed with His_6-tagged PreScission protease and dialyzed overnight against buffer containing 50 mM Tris-HCl, pH 8.0, 150 mM NaCl, 10% glycerol, and 10 mM imidazole at 4°C. Cleaved Get2CD^{Bpa}-FLAG was further purified by passing through Ni-NTA to remove the His_6 tag and His_6-PreScission protease. The purified Get2CD^{Bpa}-FLAG was collected in flowthrough and dialyzed in GET storage buffer (50 mM K-Hepes, pH 7.4, 150 mM KOAc, 5 mM Mg[OAc]$_2$, 20% glycerol, and 2 mM β-mercaptoethanol) at 4°C overnight and stored at –80°C.

Model TA substrates

The model TA substrate used for generating the Get3$^{ATTO550/-ATTO647N}$•TA complex was 3xStrep-SUMOnc-Bos1-opsin (Rao et al., 2016; Chio et al., 2019), which contains three tandem N-terminal Strep tags, a mutant yeast Smt3 with the Ulp1 cleavage site removed, residues 203–244 of the SNARE protein Bos1 encompassing its TMD, followed by a C-terminal opsin tag (GSMRMNGTEGPNMYMPMSNKTVD) to monitor the successful insertion into the ER via glycosylation. For fluorescence labeling of TA, the fourth residue (Ala) upstream of Bos1 was replaced by the amber codon to allow amber suppression with the fluorescent amino acid 7-hydroxycoumarin (described in the next section).

The model TA substrate used in the in vivo pulse-chase assay was 3xHA-BirA-Bos1TMD-opsin (abbreviated as BirA-Bos1; Cho and Shan, 2018), which contains an N-terminal 3xHA, BirA, residues 203–244 of Bos1, a GSGGS linker, and a C-terminal opsin tag. Expression of BirA-Bos1 was controlled by the GPD promotor and PGK terminator that were cloned into pRS316 (Cho and Shan, 2018).

Fluorescence labeling

Get3 with a ybbR tag (DSLEFIASKLA) inserted between residues S110 and D111 was labeled with BDP-maleimide (Thermo Fisher Scientific) or with a 1:1 mixture of ATTO550-maleimide (GE Healthcare) and ATTO 647N-maleimide (ATTO-TEC) via Sfp-catalyzed incorporation of dye-CoA conjugates (Rao et al., 2016; Chio et al., 2019, 2017b). The C-terminal His$_6$-tagged Sfp was removed through Ni-NTA affinity chromatography. The excess dye–CoA conjugates were further removed through gel filtration using a Sephadex G-25 (Sigma-Aldrich) column. Get3$^{ATTO550/ATTO647N}$-TA complex and Get3^{BDP}-TA^{Cm} were generated by in vitro translation of TA substrate 3xStrep-SUMOnc-Bos1-opsin in *E. coli* S30 cell extract (Rao et al., 2016) supplemented with Get3 variants and untagged T7 RNA polymerase and/or untagged CmRS (for generating Get3^{BDP}-TA^{Cm}). The resulting Get3-TA complex was purified using Strep-Tactin Sepharose (IBA Life Sciences; Rao et al., 2016; Chio et al., 2019).

Mini-Get1/2 was labeled with TMR-5-maleimide (Invitrogen) via thiol-maleimide reaction on an engineered single cysteine at residue S77 of Get1 or residue T34 of Get2. The labeling reaction was quenched with 1 mM DTT, and excess dye was removed using a PD-10 column packed with Sephadex G-25 resin (GE Healthcare).

Western blot

The cross-linked His-Get3×Get2CD^{Bpa}-FLAG protein band was detected by Western blot against His-Get3 and Get2CD^{Bpa}-FLAG separately. Purified His-Get3 and Get2CD^{Bpa}-FLAG variants were incubated in buffer (50 mM K-Hepes, pH 7.5, 150 mM KOAc, 5 mM Mg[OAc]$_2$, and 2 mM β-mercaptoethanol) at 0.1 μM and 20 μM (for anti-His Western blot) or 10 μM and 1 μM (for anti-FLAG Western blot) concentrations and cross-linked with UV (UVP B-100AP lamp; UVP LLC) on dry ice for 2 h or 15 min (with new lamp). The sample tubes were placed 1 cm away from the lamp source. After cross-linking, samples were separated using a 12% SDS-PAGE and analyzed by Western blot against His-Get3 using the anti-His primary antibody (Cat#A00186;

GenScript) or against Get2CD^{Bpa}-FLAG using the anti-FLAG (anti-DYKDDDDK) primary antibody (Cat#A00187; GenScript) separately. IRDye 800CW Goat anti-Mouse polyclonal IgG (H + L; Cat#925-32210; LI-COR Biosciences) was used as the secondary antibody to visualize the protein bands using the Odyssey imaging system.

Yeast cells were first treated with 0.3 M NaOH at room temperature for 3 min. After discarding the NaOH, cells were rinsed with water once and then resuspended in lysis buffer (50 mM Hepes, pH 7.4, 150 mM NaCl, 2% SDS, and 2 mM β-mercaptoethanol). Samples were then heated at 95°C for 5 min, and the supernatant was used for the further Western blot. Samples were separated using a 12% SDS-PAGE. The abundance of Get2 in yeast strains was detected by Western blot against the C-terminal FLAG tag on Get2. Model TA substrate translocation levels at steady-state in WT and Get2 variant strains were detected by anti-HA (Cat#A01244; GenScript) Western blot. Anti-PGK1 (Cat#ab197960; Abcam) Western blot was used as a loading control.

Measurements of Get3•TA-miniGet1/2 binding

All proteins and protein complexes were ultracentrifuged (TLA100; Beckman Coulter Inc.) at 100,000 rpm for 30 min at 4°C to remove aggregates before use in in vitro assays.

All fluorescence measurements were performed on a Fluorolog 3–22 spectrophotometer (HORIBA Instruments) at 25°C in GET assay buffer (50 mM K-Hepes, pH 7.4, 150 mM KOAc, 5 mM Mg[OAc]$_2$, 10% glycerol, and 1 mM DTT).

Equilibrium binding affinities between Get3^{BDP}•TA and mini-Get1/2 variants were measured by titrating 250 μl of 10 nM Get3^{BDP}•TA with increasing concentrations of TMR-labeled mini-Get1/2. Binding of mini-Get1/2 results in FRET between the BDP donor on Get3 and the TMR acceptor on mini-Get1/2. Loss of donor fluorescence was recorded using an excitation wavelength of 485 nm and emission wavelength of 517 nm, and FRET efficiency (E_{FRET}) was calculated using Eq. 1:

$$E_{FRET} = \left(1 - \frac{F}{F_0}\right) \times 100, \tag{1}$$

in which F and F_0 are the fluorescence intensity of the donor dye in the presence and absence of acceptor-labeled mini-Get1/2, respectively.

Observed E_{FRET} values were normalized by dividing with E_{max}, the FRET efficiency at saturating titrant concentrations. Normalized E_{FRET} was plotted against mini-Get1/2 concentration and fit to Eq. 2:

$$\text{Normalized } E_{FRET} = \frac{K_d + [Get3•TA] + [Get1/2] - \sqrt{(K_d + [Get3•TA] + [Get1/2])^2 - 4[Get3•TA][Get1/2]}}{2[Get3•TA]} \tag{2}$$

in which K_d is the equilibrium K_d between Get3•TA and mini-Get1/2. The Get3•TA concentration is 10 nM.

Measurements of Get3•TA dissociation

Get3•TA dissociation rates were measured by chasing 15 nM of preformed Get3^{BDP}•TA^{Cm} complexes with 3 μM mini-Get1/2 in the presence of 20 μM intein-cpSRP43, a hyperactive variant of

the cpSRP43 membrane protein chaperone that binds and traps TA substrates released from Get3. Loss of FRET between Get3[BDP] and TA[Cm] over time was monitored by following the fluorescence of TA[Cm] using an excitation wavelength of 370 nm and an emission wavelength of 450 nm. Observed time courses fit to Eq. 3:

$$F = F_e + (F_0 - F_e)e^{-k_{obsd}t}, \qquad (3)$$

in which F is the observed donor fluorescence at a particular time, F_0 is the donor fluorescence at t = 0, F_e is the donor fluorescence when the reaction is complete, and k_{obsd} is the observed rate constant of TA loss from Get3.

SEC-MALS

The S of purified mini-Get1/2 was characterized by SEC-MALS. 200 µl of 50 µM WT mini-Get1/2 was buffer-exchanged into 20 mM Tris, pH 8.0, 150 mM NaCl, and 0.02% NaN$_3$. The sample was injected onto a Superdex 75 10/300 GL column (Cytiva, formerly GE Healthcare) equilibrated in the same buffer. The chromatography column was connected with an 18-angle light-scattering detector (DAWN HELEOS II; Wyatt Technology) and a refractive index detector (Optilab t-rEX; Wyatt Technology). Data were collected every second at 25°C at a flow rate of 0.5 ml/min. The molar mass of mini-Get1/2 was then calculated using the ASTRA 6 software (Wyatt Technology).

Pulse-chase analysis of TA insertion in vivo

Yeast cells harboring the indicated Get1 or Get2 variants were transformed with the plasmid pRS316-GPD-3xHA-BirA-Bos1TMD-opsin and grown in 30 ml SD-Ura media to mid-log phase (OD$_{600}$ ~0.6) at 30°C. Cells were harvested, washed with 10 ml SD-Ura-Met-Cys media twice, resuspended in SD-Ura-Met-Cys media to a final OD$_{600}$ of 12, and incubated in a water bath at 30°C for 25 min. The remainder of the pulse-chase experiments were performed at 25°C for 5 min. Cells were pulse-labeled with 100 µCi/ml EasyTag EXPRESS35S Protein Labeling Mix (Perkin Elmer) for 2 min and chased with an equal volume of SD-Ura supplemented with 10 mM cold methionine and 1 mM cold cysteine, respectively. 450-µl aliquots of cells were removed at indicated times during chase and flash-frozen in liquid nitrogen. The 3xHA-tagged TA substrate was immunoprecipitated using anti-HA magnetic beads (Thermo Fisher Scientific) as previously described (Cho and Shan, 2018). Samples were analyzed by SDS-PAGE on 15% Tris-glycine gels and autoradiography. Successful TA insertion will lead to glycosylation at the C-terminal opsin tag in ER lumen. TA insertion efficiency was calculated using equation I$_{glycosylated}$/(I$_{glycosylated + I_{nonglycosylated}}$)%, in which "I" denotes the band intensity quantified using ImageJ from autoradiography.

µs-ALEX measurements

All protein samples were ultracentrifuged in a TLA 100 rotor (Beckman Coulter) at 100,000 rpm for 30 min at 4°C to remove aggregates before all µs-ALEX measurements. Proteins were diluted and incubated in GET assay buffer (50 mM K-Hepes, pH 7.4, 150 mM KOAc, 5 mM Mg[OAc]$_2$, 10% glycerol, and 1 mM DTT) supplemented with 0.3 mg/ml BSA during the assay.

For each measurement, fluorescently labeled Get3[ATTO550/-ATTO647N] or Get3 [ATTO550/ATTO647N]•TA was diluted to ~200 pM

final concentration and mixed with the indicated binding partners. Reactions contained 2 mM ATP or ADP, 20 µM Get1CD or Get2CD variants, or 20 µM mini-Get1/2 variants where indicated. Samples were mixed and placed either on a coverslip (for short-time measurements, i.e., up to 15 min) or in a closed chamber made by sandwiching a perforated silicone sheet (Grace Bio-Labs) with two coverslips to prevent evaporation (for long-time measurements, i.e., 30–120 min). Data were collected using an alternating-laser excitation fluorescence-aided molecule sorting setup (Kapanidis et al., 2005) with two single-photon Avalanche photodiodes (PerkinElmer) and 532-nm and 635-nm continuous wave lasers (Opto Engine LLC) operating at 135 µW and 80 µW, respectively.

µs-ALEX data analysis

All µs-ALEX data analyses were performed using FRETBursts, a Python-based open-source burst analysis toolkit for freely diffusing based smFRET (Ingargiola et al., 2016). All-photon burst search was performed to identify each burst as a minimum of 10 consecutive photons with a photon count rate at least 15-fold higher than the background rate during both the donor and acceptor excitation periods. Due to the fluctuating background rate within a measurement, the background rate was computed for every 50-s interval according to maximum likelihood fitting of the interphoton delay distribution. Dual-channel burst search (Nir et al., 2006) was performed to separate the burst species containing FRET pairs from background noise and species containing donor or acceptor only. The identified bursts were further filtered according to the following criteria: (1) $n_D^D + n_D^A \geq 15$ (exclude acceptor only species) and (2) $n_A^A \geq 15$ (exclude donor only species), where n_D^D is the number of photons detected from the donor channel during donor excitation, n_D^A is the number of photons detected from the acceptor channel during donor excitation, and n_A^A is the number of photons detected from the acceptor channel during acceptor excitation.

The values of E* and S were calculated for each burst according to the following equations:

$$E^* = n_D^A / (n_D^D + n_D^A) \qquad (4)$$
$$S = (n_D^A + n_D^D) / (n_D^D + n_A^A + n_D^A). \qquad (5)$$

The bursts with S of ~1 and ~0 represent the donor-only and the acceptor-only species, respectively. In this study, only selected bursts from the dual-channel search with S values between 0.2 and 0.8 were plotted in the FRET histogram. The accurate FRET efficiency can be calculated by applying three correction factors to E*: (1) γ-factor, the ratio between quantum yields and detection efficiency between donor and acceptor channels; (2) lk-factor, the donor spectral leakage into the acceptor channel; and (3) dir-factor, the direct excitation of acceptor by donor excitation light source. Since γ, lk, and dir are the same in the same experimental setup, and it is more accurate to fit the FRET histogram without corrections, we applied the E* values directly in the FRET histogram (Ingargiola et al., 2016). In this study, no significant change in quantum yields of donor and acceptor were observed as the local environments (e.g., binding partners, labeling positions) changed (Fig. 1, B and C). As such, the trend of

changes in E* due to the conformational changes of Get3 will match the trend of accurate FRET efficiency for each experimental condition. FRET histograms were generated by plotting E* against population distribution frequency.

BVA was performed to investigate the conformational dynamics of Get3 at the sub-millisecond time scale as previously described (Chio et al., 2017b; Torella et al., 2011). The principal idea of this analysis is to compare the empirical SD of sub-bursts (containing n consecutive photons, $n_{sub} = n_{sub}^{DD} + n_{sub}^{DA} = 5$ in this study) of any given E* within a burst due to shot noise (σ_{E*}, static limit) with observed SD of E* (SD_{E*}). SD_{E*} greater than σ_{E*} indicates FRET fluctuations due to dynamic changes in molecular conformation. For each sample, all the measured E* values were first binned with a bin width of 0.05 (20 bins total). All of the sub-bursts within bursts in each bin were used to calculate the SD_{E*} for each bin. The SD_{E*} values for each of these bins are denoted as triangles in BVA plots. To take into account the uneven numbers of bursts in each bin, a weighted dynamic score (WDS) was calculated to weight bins according to their size using Eq. 6:

$$WDS = \sqrt{\sum_{SD_{E*} - \sigma_{E*} > 0} \left(\frac{N_{E*}}{\sum N_{E*}} \right) \times (SD_{E*} - \sigma_{E*})^2}, \qquad (6)$$

where N_{E*} is the number of bursts in each bin.

To investigate the effects of Get1CD and Get2CD on dye photophysics, we analyzed the peak photon rate of donor- or acceptor-labeled Get3 in the presence of the respective ligands (Fig. S2 C). To identify signals for Donor-only species, we searched for bursts with a minimum of 10 consecutive photons detected from the donor channel at a photon count rate that is at least 15-fold higher than the background rate during the donor excitation periods. The same burst search parameters were applied to photons detected from the acceptor channel during the acceptor excitation periods to identify bursts for acceptor-only species. The bursts were further screened according to the following: for donor-only species, (1) $n_D^D \geq 50$ and (2) $S \geq 0.85$, $E \leq 0.15$; and for acceptor-only species, (1) $n_A^A \geq 50$ and (2) $S \leq 0.2$.

The mean peak count rates (MPRs, the means of individual bursts' peak photon count rates) were computed using FRET-Bursts and were used to present dye brightness.

Online supplemental material

Fig. S1 shows purification and characterization of mini-Get1/2 and Get2CD variants. Fig. S2 shows additional smFRET analysis performed in this study. Fig. S3 shows smFRET measurements of Get3 bound to the Get2CD linker deletion mutants. Fig. S4 shows Get2CD (1–150) structure predictions. Fig. S5 shows replicates for the pulse-chase assay to measure the kinetics of TA insertion into the ER in vivo.

Acknowledgments

References

Chartron, J.W., W.M. Clemons Jr., and C.J.M. Suloway. 2012. The complex process of GETting tail-anchored membrane proteins to the ER. *Curr. Opin. Struct. Biol.* 22:217–224. https://doi.org/10.1016/j.sbi.2012.03.001

Chio, U.S., H. Cho, and S.O. Shan. 2017a. Mechanisms of Tail-Anchored Membrane Protein Targeting and Insertion. *Annu. Rev. Cell Dev. Biol.* 33:417–438. https://doi.org/10.1146/annurev-cellbio-100616-060839

Chio, U.S., S. Chung, S. Weiss, and S.O. Shan. 2017b. A protean clamp guides membrane targeting of tail-anchored proteins. *Proc. Natl. Acad. Sci. USA.* 114:E8585–E8594. https://doi.org/10.1073/pnas.1708731114

Chio, U.S., S. Chung, S. Weiss, and S.O. Shan. 2019. A Chaperone Lid Ensures Efficient and Privileged Client Transfer during Tail-Anchored Protein Targeting. *Cell Rep.* 26:37–44.e7. https://doi.org/10.1016/j.celrep.2018.12.035

Cho, H., and S.O. Shan. 2018. Substrate relay in an Hsp70-cochaperone cascade safeguards tail-anchored membrane protein targeting. *EMBO J.* 37: e99264. https://doi.org/10.15252/embj.201899264

Cumberworth, A., G. Lamour, M.M. Babu, and J. Gsponer. 2013. Promiscuity as a functional trait: intrinsically disordered regions as central players of interactomes. *Biochem. J.* 454:361–369. https://doi.org/10.1042/BJ20130545

Disfani, F.M., W.L. Hsu, M.J. Mizianty, C.J. Oldfield, B. Xue, A.K. Dunker, V.N. Uversky, and L. Kurgan. 2012. MoRFpred, a computational tool for sequence-based prediction and characterization of short disorder-to-order transitioning binding regions in proteins. *Bioinformatics.* 28: i75–i83. https://doi.org/10.1093/bioinformatics/bts209

Falk, S., S. Ravaud, J. Koch, and I. Sinning. 2010. The C terminus of the Alb3 membrane insertase recruits cpSRP43 to the thylakoid membrane. *J. Biol. Chem.* 285:5954–5962. https://doi.org/10.1074/jbc.M109.084996

Fang, C., T. Noguchi, D. Tominaga, and H. Yamana. 2013. MFSPSSMpred: identifying short disorder-to-order binding regions in disordered proteins based on contextual local evolutionary conservation. *BMC Bioinformatics.* 14:300. https://doi.org/10.1186/1471-2105-14-300

Fung, H.Y.J., M. Birol, and E. Rhoades. 2018. IDPs in macromolecular complexes: the roles of multivalent interactions in diverse assemblies. *Curr. Opin. Struct. Biol.* 49:36–43. https://doi.org/10.1016/j.sbi.2017.12.007

Geng, Y., A. Kedrov, J.J. Caumanns, A.H. Crevenna, D.C. Lamb, R. Beckmann, and A.J.M. Driessen. 2015. Role of the cytosolic loop C2 and the C terminus of YidC in ribosome binding and insertion activity. *J. Biol. Chem.* 290:17250–17261. https://doi.org/10.1074/jbc.M115.650309

Gristick, H.B., M. Rao, J.W. Chartron, M.E. Rome, S.O. Shan, and W.M. Clemons Jr. 2014. Crystal structure of ATP-bound Get3-Get4-Get5 complex reveals regulation of Get3 by Get4. *Nat. Struct. Mol. Biol.* 21: 437–442. https://doi.org/10.1038/nsmb.2813

Hegde, R.S., and R.J. Keenan. 2011. Tail-anchored membrane protein insertion into the endoplasmic reticulum. *Nat. Rev. Mol. Cell Biol.* 12:787–798. https://doi.org/10.1038/nrm3226

Chio et al.
Receptor subunit cooperation drives TA targeting

Journal of Cell Biology 15 of 16
https://doi.org/10.1083/jcb.202103079

Hwang Fu, Y.H., S. Chandrasekar, J.H. Lee, and S.O. Shan. 2019. A molecular recognition feature mediates ribosome-induced SRP-receptor assembly during protein targeting. *J. Cell Biol.* 218:3307–3319. https://doi.org/10.1083/jcb.201901001

Ingargiola, A., E. Lerner, S. Chung, S. Weiss, and X. Michalet. 2016. FRET-Bursts: An Open Source Toolkit for Analysis of Freely-Diffusing Single-Molecule FRET. *PLoS One.* 11:e0160716. https://doi.org/10.1371/journal.pone.0160716

Jia, L., M. Dienhart, M. Schramp, M. McCauley, K. Hell, and R.A. Stuart. 2003. Yeast Oxa1 interacts with mitochondrial ribosomes: the importance of the C-terminal region of Oxa1. *EMBO J.* 22:6438–6447. https://doi.org/10.1093/emboj/cdg624

Jones, D.T. 1999. Protein secondary structure prediction based on position-specific scoring matrices. *J. Mol. Biol.* 292:195–202. https://doi.org/10.1006/jmbi.1999.3091

Källberg, M., H. Wang, S. Wang, J. Peng, Z. Wang, H. Lu, and J. Xu. 2012. Template-based protein structure modeling using the RaptorX web server. *Nat. Protoc.* 7:1511–1522. https://doi.org/10.1038/nprot.2012.085

Kapanidis, A.N., T.A. Laurence, N.K. Lee, E. Margeat, X. Kong, and S. Weiss. 2005. Alternating-laser excitation of single molecules. *Acc. Chem. Res.* 38:523–533. https://doi.org/10.1021/ar0401348

Kubota, K., A. Yamagata, Y. Sato, S. Goto-Ito, and S. Fukai. 2012. Get1 stabilizes an open dimer conformation of get3 ATPase by binding two distinct interfaces. *J. Mol. Biol.* 422:366–375. https://doi.org/10.1016/j.jmb.2012.05.045

Kulak, N.A., G. Pichler, I. Paron, N. Nagaraj, and M. Mann. 2014. Minimal, encapsulated proteomic-sample processing applied to copy-number estimation in eukaryotic cells. *Nat. Methods.* 11:319–324. https://doi.org/10.1038/nmeth.2834

Kutay, U., E. Hartmann, and T.A. Rapoport. 1993. A class of membrane proteins with a C-terminal anchor. *Trends Cell Biol.* 3:72–75. https://doi.org/10.1016/0962-8924(93)90066-A

Kutay, U., G. Ahnert-Hilger, E. Hartmann, B. Wiedenmann, and T.A. Rapoport. 1995. Transport route for synaptobrevin via a novel pathway of insertion into the endoplasmic reticulum membrane. *EMBO J.* 14:217–223. https://doi.org/10.1002/j.1460-2075.1995.tb06994.x

Kyte, J., and R.F. Doolittle. 1982. A simple method for displaying the hydropathic character of a protein. *J. Mol. Biol.* 157:105–132. https://doi.org/10.1016/0022-2836(82)90515-0

Liang, F.C., G. Kroon, C.Z. McAvoy, C. Chi, P.E. Wright, and S.O. Shan. 2016. Conformational dynamics of a membrane protein chaperone enables spatially regulated substrate capture and release. *Proc. Natl. Acad. Sci. USA.* 113:E1615–E1624. https://doi.org/10.1073/pnas.1524777113

Luan, H., N.C. Peabody, C.R.R. Vinson, and B.H. White. 2006. Refined spatial manipulation of neuronal function by combinatorial restriction of transgene expression. *Neuron.* 52:425–436. https://doi.org/10.1016/j.neuron.2006.08.028

Malhis, N., and J. Gsponer. 2015. Computational identification of MoRFs in protein sequences. *Bioinformatics.* 31:1738–1744. https://doi.org/10.1093/bioinformatics/btv060

Malhis, N., M. Jacobson, and J. Gsponer. 2016. MoRFchibi SYSTEM: software tools for the identification of MoRFs in protein sequences. *Nucleic Acids Res.* 44(W1):W488–W493. https://doi.org/10.1093/nar/gkw409

Mariappan, M., X. Li, S. Stefanovic, A. Sharma, A. Mateja, R.J. Keenan, and R.S. Hegde. 2010. A ribosome-associating factor chaperones tail-anchored membrane proteins. *Nature.* 466:1120–1124. https://doi.org/10.1038/nature09296

Mariappan, M., A. Mateja, M. Dobosz, E. Bove, R.S. Hegde, and R.J. Keenan. 2011. The mechanism of membrane-associated steps in tail-anchored protein insertion. *Nature.* 477:61–66. https://doi.org/10.1038/nature10362

Mateja, A., A. Szlachcic, M.E. Downing, M. Dobosz, M. Mariappan, R.S. Hegde, and R.J. Keenan. 2009. The structural basis of tail-anchored membrane protein recognition by Get3. *Nature.* 461:361–366. https://doi.org/10.1038/nature08319

Mateja, A., M. Paduch, H.Y. Chang, A. Szydlowska, A.A. Kossiakoff, R.S. Hegde, and R.J. Keenan. 2015. Protein targeting. Structure of the Get3 targeting factor in complex with its membrane protein cargo. *Science.* 347:1152–1155. https://doi.org/10.1126/science.1261671

McDowell, M.A., M. Heimes, F. Fiorentino, S. Mehmood, Á. Farkas, J. Coy-Vergara, D. Wu, J.R. Bolla, V. Schmid, R. Heinze, et al. 2020. Structural Basis of Tail-Anchored Membrane Protein Biogenesis by the GET Insertase Complex. *Mol. Cell.* 80:72–86.e7. https://doi.org/10.1016/j.molcel.2020.08.012

Mészáros, B., I. Simon, and Z. Dosztányi. 2009. Prediction of protein binding regions in disordered proteins. *PLOS Comput. Biol.* 5:e1000376. https://doi.org/10.1371/journal.pcbi.1000376

Mohan, A., C.J. Oldfield, P. Radivojac, V. Vacic, M.S. Cortese, A.K. Dunker, and V.N. Uversky. 2006. Analysis of molecular recognition features (MoRFs). *J. Mol. Biol.* 362:1043–1059. https://doi.org/10.1016/j.jmb.2006.07.087

Moll, J.R., S.B. Ruvinov, I. Pastan, and C. Vinson. 2001. Designed heterodimerizing leucine zippers with a ranger of pIs and stabilities up to 10(-15) M. *Protein Sci.* 10:649–655. https://doi.org/10.1110/ps.39401

Mukhopadhyay, R., Y.S. Ho, P.J. Swiatek, B.P. Rosen, and H. Bhattacharjee. 2006. Targeted disruption of the mouse Asna1 gene results in embryonic lethality. *FEBS Lett.* 580:3889–3894. https://doi.org/10.1016/j.febslet.2006.06.017

Nir, E., X. Michalet, K.M. Hamadani, T.A. Laurence, D. Neuhauser, Y. Kovchegov, and S. Weiss. 2006. Shot-noise limited single-molecule FRET histograms: comparison between theory and experiments. *J. Phys. Chem. B.* 110:22103–22124. https://doi.org/10.1021/jp063483n

Notredame, C., D.G. Higgins, and J. Heringa. 2000. T-Coffee: A novel method for fast and accurate multiple sequence alignment. *J. Mol. Biol.* 302:205–217. https://doi.org/10.1006/jmbi.2000.4042

Oldfield, C.J., J. Meng, J.Y. Yang, M.Q. Yang, V.N. Uversky, and A.K. Dunker. 2008. Flexible nets: disorder and induced fit in the associations of p53 and 14-3-3 with their partners. *BMC Genomics.* 9(suppl 1):S1. https://doi.org/10.1186/1471-2164-9-S1-S1

Rao, M., V. Okreglak, U.S. Chio, H. Cho, P. Walter, and S.O. Shan. 2016. Multiple selection filters ensure accurate tail-anchored membrane protein targeting. *eLife.* 5:e21301. https://doi.org/10.7554/eLife.21301

Rome, M.E., M. Rao, W.M. Clemons, and S.O. Shan. 2013. Precise timing of ATPase activation drives targeting by tail-anchored proteins. *Proc. Natl. Acad. Sci. USA.* 110:7666–7671. https://doi.org/10.1073/pnas.1222054110

Rome, M.E., U.S. Chio, M. Rao, H. Gristick, and S.O. Shan. 2014. Differential gradients of interaction affinities drive efficient targeting and recycling in the GET pathway. *Proc. Natl. Acad. Sci. USA.* 111:E4929–E4935. https://doi.org/10.1073/pnas.1411284111

Ryan, O.W., S. Poddar, and J.H.D. Cate. 2016. Crispr–cas9 genome engineering in Saccharomyces cerevisiae cells. *Cold Spring Harb. Protoc.* 2016:525–533. https://doi.org/10.1101/pdb.prot086827

Schuldiner, M., J. Metz, V. Schmid, V. Denic, M. Rakwalska, H.D. Schmitt, B. Schwappach, and J.S. Weissman. 2008. The GET complex mediates insertion of tail-anchored proteins into the ER membrane. *Cell.* 134:634–645. https://doi.org/10.1016/j.cell.2008.06.025

Shen, J., C.M. Hsu, B.K. Kang, B.P. Rosen, and H. Bhattacharjee. 2003. The Saccharomyces cerevisiae Arr4p is involved in metal and heat tolerance. *Biometals.* 16:369–378. https://doi.org/10.1023/A:1022504311669

Stefer, S., S. Reitz, F. Wang, K. Wild, Y.Y. Pang, D. Schwarz, J. Bomke, C. Hein, F. Löhr, F. Bernhard, et al. 2011. Structural basis for tail-anchored membrane protein biogenesis by the Get3-receptor complex. *Science.* 333:758–762. https://doi.org/10.1126/science.1207125

Suloway, C.J.M., J.W. Chartron, M. Zaslaver, and W.M. Clemons Jr. 2009. Model for eukaryotic tail-anchored protein binding based on the structure of Get3. *Proc. Natl. Acad. Sci. USA.* 106:14849–14854. https://doi.org/10.1073/pnas.0907522106

Szyrach, G., M. Ott, N. Bonnefoy, W. Neupert, and J.M. Herrmann. 2003. Ribosome binding to the Oxa1 complex facilitates co-translational protein insertion in mitochondria. *EMBO J.* 22:6448–6457. https://doi.org/10.1093/emboj/cdg623

Torella, J.P., S.J. Holden, Y. Santoso, J. Hohlbein, and A.N. Kapanidis. 2011. Identifying molecular dynamics in single-molecule FRET experiments with burst variance analysis. *Biophys. J.* 100:1568–1577. https://doi.org/10.1016/j.bpj.2011.01.066

van der Lee, R., M. Buljan, B. Lang, R.J. Weatheritt, G.W. Daughdrill, A.K. Dunker, M. Fuxreiter, J. Gough, J. Gsponer, D.T. Jones, et al. 2014. Classification of intrinsically disordered regions and proteins. *Chem. Rev.* 114:6589–6631. https://doi.org/10.1021/cr400525m

Wang, F., E.C. Brown, G. Mak, J. Zhuang, and V. Denic. 2010. A chaperone cascade sorts proteins for posttranslational membrane insertion into the endoplasmic reticulum. *Mol. Cell.* 40:159–171. https://doi.org/10.1016/j.molcel.2010.08.038

Wang, F., A. Whynot, M. Tung, and V. Denic. 2011. The mechanism of tail-anchored protein insertion into the ER membrane. *Mol. Cell.* 43:738–750. https://doi.org/10.1016/j.molcel.2011.07.020

Yin, J., A.J. Lin, D.E. Golan, and C.T. Walsh. 2006. Site-specific protein labeling by Sfp phosphopantetheinyl transferase. *Nat. Protoc.* 1:280–285. https://doi.org/10.1038/nprot.2006.43

Young, T.S., I. Ahmad, J.A. Yin, and P.G. Schultz. 2010. An enhanced system for unnatural amino acid mutagenesis in E. coli. *J. Mol. Biol.* 395:361–374. https://doi.org/10.1016/j.jmb.2009.10.030

Zalisko, B.E., C. Chan, V. Denic, R.S. Rock, and R.J. Keenan. 2017. Tail-anchored protein insertion by a single Get1/2 heterodimer. *Cell Rep.* 20:2287–2293. https://doi.org/10.1016/j.celrep.2017.08.035
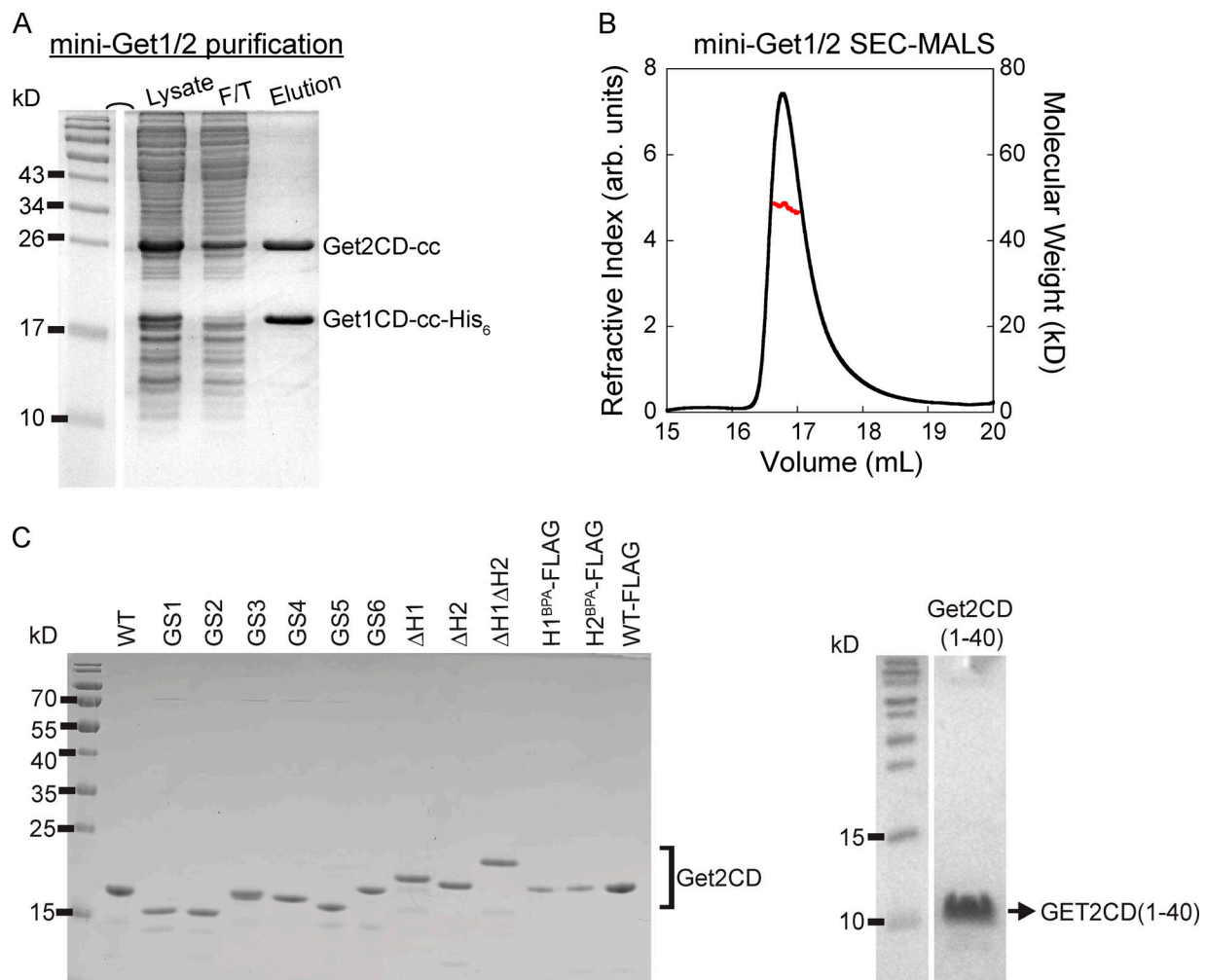
Figure S1. **Purification and characterization of mini-Get1/2 and Get2CD variants.** Related to Figs. 1 and 5. **(A)** Recombinant mini-Get1/2 was expressed in BL21(DE3)* cells and purified using Ni-NTA chromatography followed by size exclusion chromatography (see Materials and methods). The resulting complex consists of Get2CD (residues 1–150) and C-terminally His$_6$-tagged Get1CD (residues 22–102) fused to complementarily charged α-helices that form a stable cc. Related to Fig. 1. **(B)** SEC-MALS analysis of purified mini-Get1/2 indicates a molecular weight of ∼45 kD, confirming that it is a heterodimer. Related to Fig. 1. **(C)** Coomassie blue-stained SDS PAGE gel of purified Get2CD variants. Related to Fig. 5. F/T, Ni flowthrough.

Figure S2. **Additional smFRET analysis performed in this study.** Related to Figs. 1, 2, 3, 4, 5, and 6. **(A and B)** Structures of *open* Get3 bound to Get1CD (A, PDB 3SJA) and *closed* Get3 bound to Get2CD N-terminal helix (B, PDB 3ZS9). Each Get3 dimer (light and dark gray) in the structures binds with two Get1CDs (purple) or two Get2CDs (blue). The identified Get3 binding sites on Get1CD and Get2CD are depicted as black bars in the primary structures (top). The residues mutated to cystine for TMR labeling in Get1/2 CDs are shown in red in both the primary and crys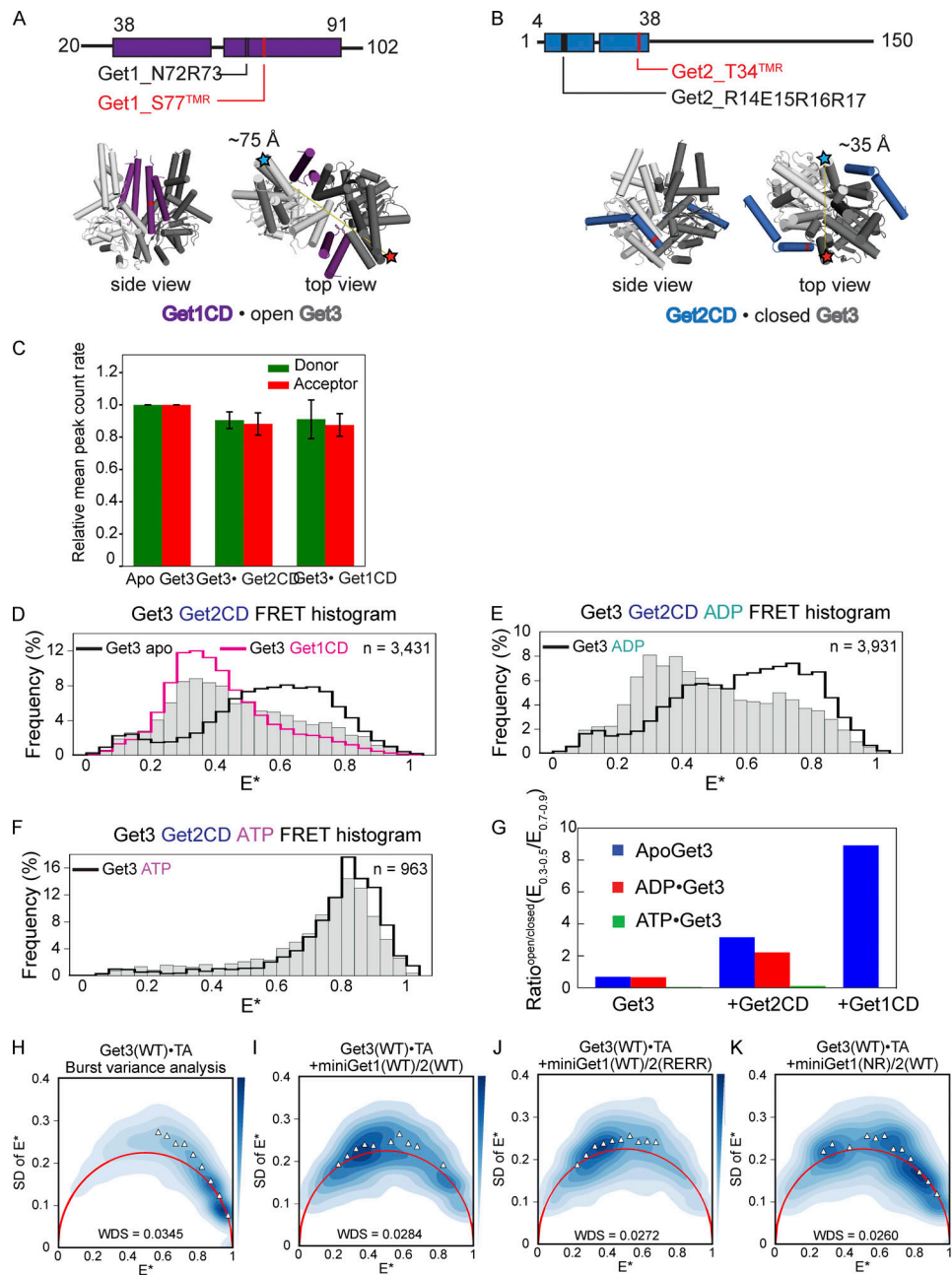tal structure (related to Figs. 1 and 6). The labeling sites on Get3 for the smFRET measurement (related to Figs. 3, 4, and 5), TA release (related to Fig. 2), and Get1/2 binding (related to Figs. 1 and 6) are shown as stars on the top view of the crystal structures. The predicted distances between the two labeling sites on Get3 are 75 Å and 35 Å in the open and closed conformations, respectively. **(C)** Get1CD and Get2CD do not significantly affect the brightness of the donor (ATTO550, green) and acceptor (ATTO647N, red) dye labeled on Get3, as measured by the relative MPRs. Compared with apo-Get3, the MPR of the donor dye decreases by 9.4% and 8.9% upon Get3 binding with Get2CD and Get1CD, respectively; the MPR of the acceptor dye decreased by 11.8% and 12.5% upon Get2CD and Get1CD binding, respectively. Error bars denote SD for measurements from four different days. **(D–F)** smFRET measurements using Get3 labeled by the Cy3B/ATTO647N dye pair (donor/acceptor). The smFRET histograms of Get3 bound to Get2CD in the absence (D) and presence of 2 mM ADP (E) or 2 mM ATP (F) are shown as gray bars. Saturating Get2CD (10 µM) was added where indicated. The smFRET histograms of free Get3 (black outline) and Get3 bound to Get1CD (pink outline) in the respective nucleotide states are shown for comparison. "n" denotes the number of bursts used to generate the smFRET histogram. Related to Fig. 3. **(G)** Quantification of the smFRET histograms from D–F. The degree of Get1/2 CD–induced Get3 opening (Ratio$_{open/closed}$) is semi-quantitatively calculated from the ratio of Get3 bursts in the low FRET bins ($E^* = 0.24$–0.4) to that in the high FRET bins ($E^* = 0.72$–0.88). Related to Fig. 3. **(H–K)** smFRET BVA analyses of Get3•TA in the absence (H) and presence of WT mini-Get1/2 (I), mini-Get1/2(RERR) (J), and mini-Get1(NR)/2 (K). Saturating (3 µM) mini-Get1/2 was used in all experiments. "n" denotes the number of bursts used to generate each FRET histogram. The red curve in BVA analyses represents the SD expected for shot-noise-limited E^*. Triangles denote SDs of all sub-bursts within each E^* bin, which were used to calculate the weighted dynamic score (WDS). Related to Fig. 4.
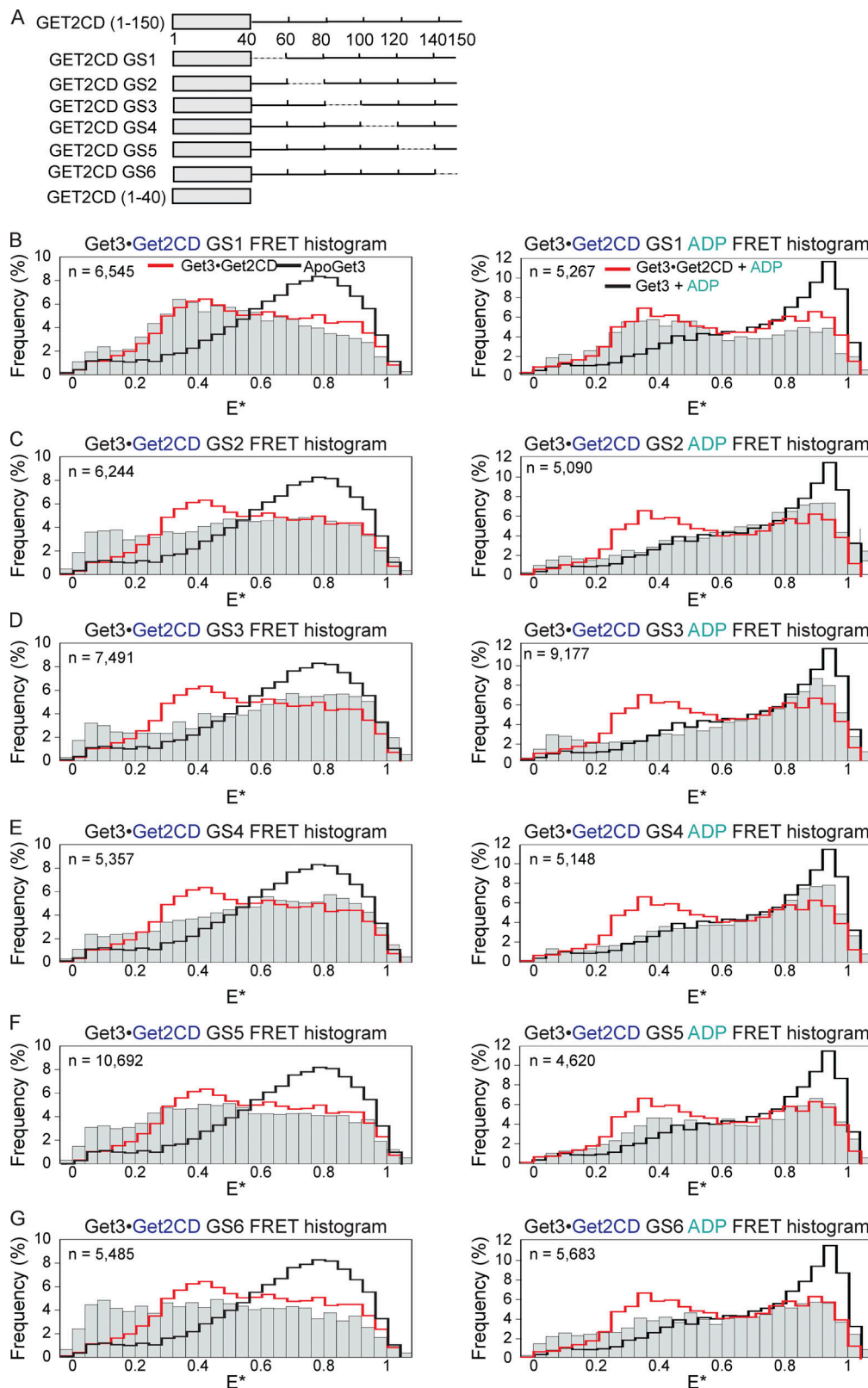
Figure S3.   **smFRET measurements of Get3 bound to the Get2CD linker deletion mutants.** Related to Fig. 5. **(A)** Schematic representation of the Get2CD linker mutants. Dashed lines denote the sequence SGGSGSGSGSSG that replaces the indicated region except for GET2GS6, in which the dashed line represents the sequence GSGSGS. Numbers denote the residues in ScGet2. **(B–G)** The smFRET histograms of Get3 bound to the indicated Get2CD linker mutants in the absence (left) and presence (right) of 2 mM ADP are shown as gray bars. The histograms of free Get3 (black outline) and Get3 bound to WT Get2CD (red outline) in the corresponding nucleotide states are shown for comparison. "n" denotes the number of bursts analyzed to generate the FRET histogram. Saturating Get2CD (20 µM) was used in all measurements.

Figure S4. **Get2CD (1–150) structure predictions.** Related to Fig. 5. **(A)** Secondary structure prediction of Get2CD using RaptorX (http://raptorx.uchicago.edu/StructPredV2/predict/). Blue and purple bars highlight H1 and H2, respectively. **(B)** Secondary structure prediction of Get2CD using the PSIPRED webserver (http://bioinf.cs.ucl.ac.uk/psipred/), which predicts protein secondary structure based on position-specific scoring metrics generated from Position-Specific Iterated BLAST. Blue and purple bars highlight H1 and H2, respectively. **(C)** Sequence alignment of Get2CD(1–151) using the T-COFFEE server (http://tcoffee.crg.cat/apps/tcoffee). The blue and purple bars highlight H1 and H2, respectively. cons., consensus.

Chio et al.
Receptor subunit cooperation drives TA targeting

Journal of Cell Biology
https://doi.org/10.1083/jcb.202103079

S4

A

| | | 1 | 2 | 3 | 4 | 5 | 6 | 7 |

Endo H — + — + — + — + — + — + — +

replicate1: TA-glyc —
TA
translocation%   92   96   81   84   96   94   93

—40kD

replicate 2: TA-glyc —
TA
translocation%   93   96   81   79   93   95   96

—40kD

B

Get1WT / Get2WT (×8)

chase time (min): 0 1 2 5 0 1 2 5 0 1 2 5 0 1 2 5 0 1 2 5 0 1 2 5 0 1 2 5 0 1 2 5

TA-glyc —
TA —

—40kD

Get1WT / Get2ΔH1 (×7)

chase time (min): 0 1 2 5 0 1 2 5 0 1 2 5 0 1 2 5 0 1 2 5 0 1 2 5 0 1 2 5

TA-glyc —
TA —

—40kD

Get1WT / Get2ΔH2 (×6)

chase time (min): 0 1 2 5 0 1 2 5 0 1 2 5 0 1 2 5 0 1 2 5 0 1 2 5

TA-glyc —
TA —

—40kD

Get1WT / Get2ΔH1ΔH2 (×5)

chase time (min): 0 1 2 5 0 1 2 5 0 1 2 5 0 1 2 5 0 1 2 5

TA-glyc —
TA —

—40kD

Get1NR / Get2WT (×3)

chase time (min): 0 5 10 15 0 5 10 15 0 5 10 15

TA-glyc —
TA —

—40kD

Get1WT / Get2RERR (×3)

chase time (min): 0 5 10 15 0 5 10 15 0 5 10 15

TA-glyc —
TA —

—40kD

C

1 2 3 4 5 6 7

40—
35—

anti-FLAG] replicate1
anti-PGK1

40—
35—

anti-FLAG] replicate 2
anti-PGK1

kD   1 1.25 0.9 1.4 1.3 1.7   Get2 relative exression level
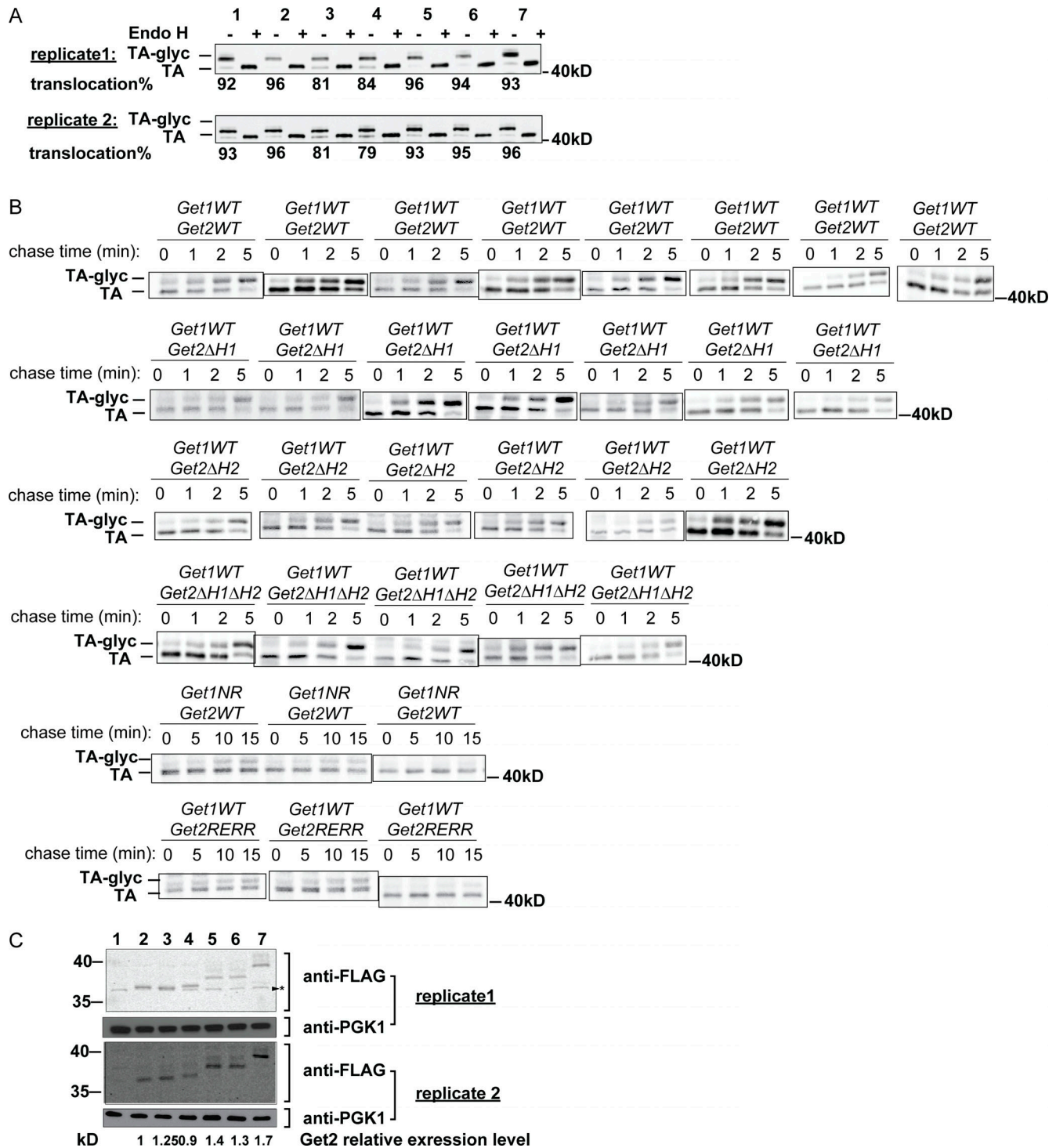
Figure S5.   **Replicate for the pulse-chase assay to measure the kinetics of TA insertion into the ER in vivo.** Related to Fig. 8. **(A)** Model TA substrate translocation levels at steady-state in WT and Get2 variant strains. TA substrates were detected by anti-HA Western blot. The glycosylated (TA-glyc) and nonglycosylated (TA) proteins were confirmed by endoglycosidase H (Endo H) treatment. Translocation efficiencies were quantified below the blot images. Lanes 1–7 are loaded with the lysate from the yeast strains: BY4741 WT (lane 1), GET2-FLAG (lane 2), GET2-FLAG get1NR (lane 3), get2RERR-FLAG (lane 4), get2ΔH1-FLAG (lane 5), get2ΔH2-FLAG (lane 6), and get2ΔH1ΔH2-FLAG (lane 7). **(B)** SDS-PAGE autoradiography of replicates for the pulse-chase assay to measure TA insertion. The gel images from the first column of each strain are the representative autoradiographs shown in Fig. 8. **(C)** The abundance of Get2 in yeast strains was detected by Western blot against the C-terminal FLAG tag on Get2. All strains were generated using yeast CRISPR-Cas9 genome editing. Anti-PGK1 Western blot was used as a loading control. The values below the image indicate the relative Get2 expression levels in replicate 2. "*" denotes a nonspecific band detected by the anti-FLAG antibody. The samples in lanes 1–7 are the same as those in the respective lanes in A.